Title: Blocking SHP2 benefits FGFR2 inhibitor and overcomes its resistance in FGFR2-amplified gastric cancer

Yue Zhang[1], Hanbing Wang[1], Yutao Wei[2], Yunfeng Pan[1], Xueru Song[1], Tao Shi[1], Jie Shao[1], Lixia Yu[1], Baorui Liu[1], Yue Wang[1*], Jia Wei[1,3,4*]

[1]Department of Oncology, Nanjing Drum Tower Hospital, Affiliated Hospital of Medical School, Nanjing University, Nanjing, China

[2]Nanjing Drum Tower Hospital Clinical College of Traditional Chinese and Western Medicine, Nanjing University of Chinese Medicine, Nanjing, China

[3]Chemistry and Biomedicine Innovation Center (ChemBIC), Nanjing University, Nanjing, China

[4]Collaborative Innovation Center for Personalized Cancer Medicine, Nanjing Medical University, Nanjing, China

Jia Wei and Yue Wang contributed equally to this article.

Corresponding Author:

Jia Wei, M.D., Ph.D., Department of Oncology, Nanjing Drum Tower Hospital, Affiliated Hospital of Medical School, Nanjing University, Nanjing, China. Email: jiawei99@nju.edu.cn.; Yue Wang, M.D., Ph.D., Department of Oncology, Nanjing Drum Tower Hospital, Affiliated Hospital of Medical School, Nanjing University, Nanjing, China. Email: wangyue2012nju@163.com.

Abstract

Fibroblast growth factor receptor 2 (FGFR2) is an important member of receptor tyrosine kinase (RTK) family. FGFR2 amplification occurs at a high frequency in gastric cancer (GC) and has been proven to be closely associated with poor prognosis and insensitivity to chemotherapy or immunotherapy. Current FGFR2-targeted therapies have limited efficacy. Hence, how to enhance efficacy and reverse resistance are urgent problems clinically. Src homology region 2-containing protein tyrosine phosphatase 2 (SHP2) serves as the shared downstream mediator of all RTKs and a prominence immunosuppressive molecule. In this study, we identified FGFR2 amplification in 6.2% (10/161) of GC samples in our center. Then we showed that dual blocking SHP2 and FGFR2 enhanced the effects of FGFR2 inhibitor (FGFR2i) in FGFR2-amplified GC both *in vitro* and *in vivo* via suppressing RAS/ERK and PI3K/AKT pathways. We further showed that it overcame FGFR2i resistance by reversing the feedback activation mediated by other RTKs and continuously suppressing FGFR2-initiated downstream pathways. Notably, SHP2 blockade could suppress PD-1 expression and promoted IFN-γ secretion of $CD8^+$ T cells, enhancing the cytotoxic functions of T cells in tumor immune microenvironment. Overall, our findings suggest that dual blocking SHP2 and FGFR2 is a compelling rationale with both targeted treatment and immune regulation for FGFR2-amplified GC.

Key words: FGFR2; SHP2; Gastric cancer; Targeted therapy

Impact statement: Dual blocking SHP2 and FGFR2 can not only promote the targeted tumor-killing effects and overcome FGFR2 inhibitor resistance caused by feedback activation, but also activate T cell-mediated anti-tumor immunity by inhibiting PD-1 pathway in FGFR2-amplified GC.

Funding information: This work was funded by grants from the National Natural Science Foundation of China (82373263, China); The provincial key medical disciplines during the “14th Five-Year Plan” period (ZDXK202233, China); Jiangsu

Provincial Natural Science Foundation Youth Project (BK20230151, China) and the Wu Jieping Medical Foundation Special Fund for Targeted Cancer Therapy (Youth Research Project) (320.6750.2023-11-30, China).

Introduction

Gastric cancer (GC) ranks as the third leading cause of cancer death globally(Ajani et al., 2022; Smyth et al., 2020; Wei et al., 2020). Due to the absence of specific early signs, over 70% of GC patients are diagnosed at an advanced stage(Guan et al., 2023; Song et al., 2017). Concurrently, treatments for advanced GC predominantly include chemotherapy, targeted therapy, radiotherapy and immunotherapy. Anti-programmed cell death protein 1 (PD-1) antibody nivolumab plus chemotherapy has been approved by Food and Drug Administration (FDA) as the standard first-line treatment for advanced GC(Janjigian et al., 2021; Smyth et al., 2020; Zhao et al., 2022). Meanwhile, the Cancer Genome Atlas (TCGA) has classified GC patients into four subtypes including Epstein Barr virus (EBV) type, Microsatellite Instability (MSI) type, Genomic stability (GS) type and chromosomal instability (CIN) type("Comprehensive molecular characterization of gastric adenocarcinoma," 2014). Among them, EBV and MSI types are more likely to benefit from immunotherapies, while CIN and GS types tend to be less responsive. Fortunately, the unique composition structure of CIN type provides potential anti-tumor targets. CIN type is in the majority, accounting for about 50%, with distinct aneuploidy and focal amplification of receptor tyrosine kinases (RTKs) as its molecular feature("Comprehensive molecular characterization of gastric adenocarcinoma," 2014). RTKs are common tumor-driven genes, including human epidermal growth factor receptor 2 (HER-2), fibroblast growth factor receptor 2 (FGFR2), epidermal growth factor receptor (EGFR) and so on(Du & Lovly, 2018; Paul & Hristova, 2019). The combination of anti-HER-2 antibody Trastuzumab and chemotherapy has been approved by FDA as the first-line treatment for HER-2 positive advanced GC(Kang, 2023; Smyth et al., 2020; Yang et al., 2020). In the meantime, other RTKs, especially FGFR2, have also displayed huge potential as anti-tumor targets.

FGFR2 is also a representative member of the RTK family. Several studies have documented that FGFR2 blockade can inhibit the occurrence and development of malignant tumors by regulating PI3K/AKT, RAS/ERK and JAK/STAT pathways(Babina & Turner, 2017; Gordon et al., 2022; Katoh & Nakagama, 2014). It's worth noting that FGFR2 amplification has been identified in up to 7.7% of advanced GC patients(Jogo et al., 2021), and is closely associated with poor prognosis and limited response to chemotherapy and immunotherapy(Ahn et al., 2016; Hur et al., 2020; Kim, Kim, Jang, et al., 2019; Koh et al., 2019). Currently, there've been several approaches for FGFR2 inhibition in FGFR2-amplified GC. For instance, Bemarituzumab (FPA144) is a specific anti-FGFR2b monoclonal antibody(Katoh et al., 2024), However, in a phase II clinical trial (NCT03694522), it has been demonstrated that Bemarituzumab monotherapy didn't statistically significantly improve progression-free survival (PFS) in FGFR2b-selected GC patients(Wainberg et al., 2022). Besides, small molecule inhibitors targeting FGFR2 are also primary methods for FGFR2-amplified GC treatment. In a previous phase II clinical trial (NCT01795768), FGFR2 inhibitor AZD4547 achieved an overall response rate (ORR) of 33% in patients with previously treated advanced FGFR2-amplified gastroesophageal cancer, and a median PFS of responding patients of 6.6 months(Pearson et al., 2016). Based on its distinguished therapeutic effects, AZD4547 was granted by FDA as an orphan drug for GC. However, subgroup analysis indicated that robust single-agent response to AZD4547 was only observed in high-level FGFR2-amplified cancers in this trial(Pearson et al., 2016). And in another phase II clinical trial (NCT01457846), AZD4547 failed to significantly improve patients' PFS compared to paclitaxel (3.5 months vs 1.8 months, P=0.9581) as a second-line treatment for advanced gastric adenocarcinoma(Van Cutsem et al., 2017). Given that inhibiting FGFR2 alone is often difficult to achieve ideal therapeutic effects, identifying suitable combinations is crucial to the treatment of FGFR2-amplified GC.

Although RTK targeted therapies have been proved to have certain anti-tumor therapeutic effects, drug resistance of RTK inhibitors remain a common problem. One of the main reasons for RTK inhibitors resistance is the activation of downstream

signaling pathways mediated by bypass RTKs. Previous researches have revealed that the downstream pathway feedback upregulation caused by EGFR activation leaded to FGFR2 inhibitor resistance in intrahepatic cholangiocarcinoma (iCCA) with FGFR2 fusion(Wu et al., 2022). Src homology region 2-containing protein tyrosine phosphatase 2 (SHP2) is the common downstream factor of RTKs including FGFR2, acting as a central node between FGFR2 and PI3K/AKT, RAS/ERK or JAK/STAT pathways(Chen et al., 2016; Sodir et al., 2023). As the shared molecule downstream of all RTKs, SHP2 inhibitor and its combination with RTK inhibitors were reported to be ideal strategies for treating a large class of RTK-driven cancers, including EGFR-amplified, KRAS-amplified, KRAS G12C-mutanted cancers and so on(Chen et al., 2016; Fedele et al., 2021; Wong et al., 2018). Therefore, we speculate that the combination of FGFR2 inhibitor and SHP2 inhibitor is likely to alleviate FGFR2 inhibitor resistance by inhibiting the feedback activation of bypass RTK pathways.

Meanwhile, SHP2 is also a significant downstream molecule of PD-1(Chen et al., 2016; Song et al., 2022). SHP2 has been proved to suppress T cell activation by inactivating TCR and CD28 signaling(Li et al., 2015), which are two costimulatory signals mediating T cell development and maturation(Ai et al., 2020; Liu et al., 2020). Numerous preclinical studies have revealed that SHP2 inhibition can inhibit tumors by enhancing anti-tumor immunity(Liu et al., 2017; Zhao et al., 2019). Accordingly, we suppose that simultaneously blocking FGFR2 and SHP2 has the potential to suppress tumor growth through both targeted intervention and immune activation.

Overall, we aim to explore the combined anti-tumor capacity and potential mechanisms of co-inhibiting FGFR2 and SHP2 in FGFR2-amplified GC, providing a “two-pronged” combination therapy mode with targeted and immune dual effects for GC patients with FGFR2 amplification.

Methods

Patient samples and next-generation sequencing

We collected gastroscopy biopsy or surgically collected specimens of 161 GC patients from January 2016 to August 2023 in Nanjing Drum Tower Hospital. Next-generation

sequencing (NGS) and analysis were performed in OrigiMed (Shanghai, China) based on 450 YuanSu^{TM} gene panel. At least 50 ng DNA were extracted from Formalin fixed paraffin-embedded (FFPE) tumor tissues using QIAamp DNA FFPE Tissue Kit. Genes capture and sequencing were performed at a mean depth of 1000× by Illumina NextSeq 500 (San Diego, CA, USA). Gene alterations, including substitution, gene amplification, gene homozygous deletion, gene fusion and truncation were evaluated. Tumor mutation burden (TMB) was estimated by calculating somatic non-synonymous mutations per megabase in each patient. The study was carried out in compliance with the code of ethics of the World Medical Association (Declaration of Helsinki) and approved by the Ethics Committee of Nanjing Drum Tower Hospital (No. 2021-324-01).

Mice

Four to six-week-old female BALB/c nude mice were purchased from GemPharmatech Co. Ltd. Mice were kept in specific pathogen-free animal facilities at the Comprehensive Cancer Centre of Nanjing Drum Tower Hospital.

Cells

Human GC cell line KATOIII was donated from Nanjing University Chao Yan laboratory. Human GC cell lines SNU-16 (ATCC CRL-5974), MKN45 (KANGBAI CBP60488), NUGC4 (KANGBAI CBP60493), HGC27 (KANGBAI CBP60480) and SNU601 (KANGBAI CBP60507) were purchased from the Cell Bank of the Chinese Academy of Sciences (Shanghai, China). All cells were cultured in Roswell Park Memorial Institute (RMPI) 1640 medium supplemented with 10% fetal calf serum (FBS) and 1% penicillin-streptomycin at 37℃ with 5% CO_2. Primary GC cells were derived from ascites of a FGFR2-amplified GC patient who was resistant to FGFR2 inhibitors. Primary human peripheral blood mononuclear cells (PBMCs) were separated from human peripheral blood donated by 2 healthy people by Ficoll (TBD, LTS1077) and induced by 80 IU/ml IL-2 (Pepro Tech, 200-02). Human sample used in this study obtained the patients' consent and the approval of the Ethics Committee of Nanjing Drum Tower Hospital (No. 2021-324-01).

CCK-8 assay

Cell Counting Kit-8 (CCK-8) (Vazyme, A311-01/02) assay was used to evaluate the effects of AZD4547 (Selleck, S2801), SHP099 (MedChemExpress, HY-100388) and combination administration on cancer cell proliferation. 3000 GC cells were seeded in 96-well plates with 100 μl of 10% FBS 1640 medium, and treated with SHP099, AZD4547 or combination therapy on the 2rd day. After 4 days incubation, 10 μl CCK-8 was added into each well and incubated for 2h. Asorbance was measured at 450 nm with microplate reader. Cell viability=[(OD_Drug-OD_Blank)/(OD_Control-OD_Blank)]×100%.

Cell apoptosis analysis

Annexin V-FITC/PI Apoptosis Detection Kit (Vazyme, A211-01) was used to detect drug effects on cancer cell apoptosis. GC cells were seeded in 12-well plates at a density of 1×10^5 cells per well and incubated with different formulations for 2 days. Afterwards, cells were collected and suspended in 100 μl binding buffer containing 2.5 μL Annexin V-FITC and 2.5 μL propidium iodide (PI) for 10 min in the darkness. Samples were run by flow cytometer and analyzed by FlowJo (RRID:SCR_008520).

Western blotting

SNU-16 and KATOIII were seeded in 6-well plates at a density of 5×10^5 cells per well with 10% FBS 1640 medium, and were incubated with SHP099, AZD4547 or combination therapy for 1 hour or 2 days. Primary human tumor cells derived from ascites of a FGFR2-amplified GC patient were incubated with different administrations for 1 hour. Mouse tumor tissues were collected after 6 hours of last drug administration and homogenized after snap freezing. Then tumor tissues and cells were lysed in cell lysis buffer (NCM Biotech, WB3100) containing 1% protease and phosphatase inhibitors (NCM Biotech, P002). 10 μg of protein was used to detect the expression levels of FGFR2-initiated downstream signaling molecules by SDS-PAGE, electro-transfer and immunoblotting with specific antibodies. The following antibodies were used: from Cell Signaling Technology, phospho-FGFR Tyr653/654 (Cell Signaling Technology Cat# 3476, 1:1000), SHP2 (3397T, 1:2000), phospho-SHP2 Tyr542 (3751T, 1:1000), ERK1/2 (4695T, 1:1000), phospho-ERK1/2 Thr202/Tyr204 (4370T, 1:2000), p38 (8690T, 1:1000), phospho-p38 Thr180/Tyr182

(4511T, 1:1000), AKT (9272S, 1:1000), phospho-AKT Ser473 (4060S, 1:2000), mTOR (2983T, 1:1000), phospho-mTOR Ser2448 (5536S, 1:1000), GAPDH (5174S, 1:1000), Anti-mouse IgG, HRP-linked Antibody(7076P2, 1:2000); from Santa Cruz Biotechnology, FGFR2 (sc-6930, 1:500); from Biosharp, Goat Anti-Rabbit IgG, HRP-linked Antibody(BL003A, 1:5000).

Cell surface marker staining

PBMCs were incubated with different therapies in the presence of 0.25 μg/ml human anti-CD3 antibody (InVivoMAb, #BE0001-2) and 1 μg/ml human anti-CD28 antibody (InVivoMAb, #BE0248) for 24 hours, and then stained with FITC-anti-CD8 (BD Biosciences, 555634), Percp-Cy5.5-anti-CD4 (Biolegend, 317428) and PE-anti-PD-1 (Biolegend, 329906) for 30 min. Samples were run by flow cytometer. The cellular supernatants were collected and detected by Cytometic Beed Array (CBA) human IFN-γ kit (BD Biosciences, 558456).

Intracellular staining

The intracellular interferon-γ (IFN-γ) expression in $CD8^+$ T cells was detected by a BD Biosciences intracellular staining kit according to the instructions. After different processing for 24 hours, PMBCs were firstly stained with FITC-anti-CD8 and Percp-Cy5.5-anti-CD4 on cell surface for 30 min, and then stained with PE-IFN-γ after fixation and permeabilization. Samples were then run by flow cytometer and analyzed by FlowJo (RRID:SCR_008520).

Cytotoxicity assay

To evaluate the tumor-killing capacity of drug-stimulated T cells in vitro, T cells were pretreated with different formulations for 2 days. SNU-16 cells labled with carboxyfluorescein succinimidyl ester (Sigma, 21888) were seeded into ultralow 96-well plates at a density of 2×10^4 cells per well as the target cells. Drug-stimualted T cells were then added into the well at an E:T ratio of 10:1, 20:1, 40:1 as the effector cells and incubated with target cells for 9h. Afterwards, cells were staind with propidium iodide (Sigma, 537059) for 10 min in the darkness and analyzed with flow cytometer.

Syngeneic mouse tumor models

Four to six-week-old female BALB/c nude mice (T cell deficient) were subcutaneously injected with 1×10^7 SNU-16 cells suspended in 100 μL PBS with 50% Matrigel (BD Biocoat, 356234). When the tumor volume reached approximately 100-150 mm^3, mice were randomized into 4 groups (n=5 per group) and started on treatment with PBS, SHP099 50 mg/kg, AZD4547 1.56 mg/kg, SHP099 50 mg/kg plus AZD4547 1.56 mg/kg. The dosage of medications used in animal experiments referred to previous researches(Wong et al., 2018; Xie et al., 2013). Drugs were delivered by oral gavage every day for 21 days. Tumor dimensions were measured every other day and tumor size was calculated as $0.5 \times \text{length} \times \text{width}^2$. All mice were killed on day 28 after tumor implantation. Tumor tissues were harvested for further analysis. All animal experiments were approved by the Institutional Animal Care and Use Committee of Drum Tower Hospital (approval number: 2022AE01029).

Statistical analysis

GraphPad Prism (RRID:SCR_002798) was used to conduct statistical analysis and construct graphics. Data are presented as the means ± standard error of the mean (SEM) and compared by unpaired t test, linear regression t test, Welch's t test, Pearson's Chi-square test, Fisher's exact test, Wilcoxon Test, ordinary one-way ANOVA or two-way ANOVOA. $P < 0.05$ was considered statistically significant. ns, not significant; *P < 0.05, **P < 0.01, ***P < 0.001 and ****P < 0.0001.

Results

Recurrent FGFR2 gene amplification in Chinese GC patients

161 GC samples collected from Nanjing Drum Tower Hospital were performed with NGS. The top 5 most significantly altered genes were TP53 (61%), ARID1A (25%), CDH1 (16%), ERBB2 (12%) and PIK3CA (12%) (Fig. S1A). Meanwhile, CCNE1 (8%), ERBB2 (7%), FGFR2 (6%), MET (6%) and CCND1 (6%) were the top 5 most frequently amplified genes in the cohort (Fig. 1A). Notably, the proportion of FGFR2 amplification ranked third after CCNE1 and ERBB2 among all amplified genomes (Fig. 1A). We can find FGFR2-amplified GC patients also occupied quite a high portion in TCGA-STAD cohort (15/295; 5%) (Fig. 1B), further emphasizing the

prevalence of FGFR2-amplified GC patients.

Moreover, in our cohort, patients with FGFR2 amplification tended to present later TNM stages, although not statistically significant in difference (Fig. S1B-D). Also, Patients harboring FGFR2 amplification in TCGA exhibited higher FGFR2 mRNA expression levels ($P<0.0001$) (Fig. 1C). And, FGFR2 mRNA expression showed a positive correlation with PTPN11 mRNA expression ($P=0.0496$, $R^2=0.01468$) (Fig. 1D), the chief coding gene of SHP2, suggesting a potential co-overexpression of SHP2 in patients with FGFR2 amplification.

SHP099 enhances the anti-tumor effects and overcomes the resistance of FGFR2 inhibitors in FGFR2-amplified GC

FGFR2-amplified GC cell lines SNU-16 and KATOIII were detected to exhibit relatively higher FGFR2 expression levels compared to other human GC cell lines (Fig. S2). Then, the anti-tumor capacity of FGFR2 inhibitor, SHP2 inhibitor monotherapy or combination therapy was detected *in vitro*. It demonstrated that the combination administration of AZD4547 and SHP099 significantly suppressed cell proliferation compared to AZD4547 monotherapy in both KATOIII ($P<0.0001$) and SNU-16 ($P<0.0001$) (Fig. 2A and B). Moreover, in groups treated with high concentration of AZD4547, the combination therapy notably enhanced cancer cell apoptosis in both KATOIII ($P=0.0001$ Combo vs. SHP099; $P<0.0001$ Combo vs. AZD4547) and SNU-16 ($P<0.0001$ Combo vs. SHP099; $P=0.0017$ Combo vs. AZD4547) (Fig. 2C and D). The above results confirm that the combination of SHP099 and AZD4547 has a synergistic effect on tumor cell killing and apoptosis in FGFR2-amplified GC *in vitro*.

To unravel the mechanisms underlying the anti-tumor effects of combination therapy, we investigated the expression levels of key proteins of PI3K/AKT and MAPK pathways in KATOIII following drug treatment for 1 hour or 48 hours. While the combination of 3nM AZD4547 and 10 μM SHP099 might not have led to a stronger inhibition of phospho-FGFR and phospho-SHP2 compared to 10 nM AZD4547 single-agent treatment, it induced a more pronounced suppression of downstream

signal pathways of FGFR2, particularly phospho-ERK1/2 (Fig. 2E). Interestingly, levels of phospho-p38, which is a crucial cascade mediating another MAPK pathway(Lee et al., 2020), remained unaffected by the medication. It's worth noting that although phospho-FGFR and phospho-SHP2 were further suppressed over time, AZD4547 single-agent treatment failed to sustain downstream signal suppression after 48 hours. In contrast, the combination treatment could continuously inhibit the downstream signaling molecules and overcome the feedback activation caused by prolonged treatment duration. Similar regulations of these phospho-proteins were also observed in another FGFR2-amplified GC cell line SNU-16 (Fig. 2F).

The synergistic efficacy of combining AZD4547 with SHP099 in primary tumor cells derived from a FGFR2 inhibitor-resistant GC patient

A 49-year-old Asian female was diagnosed with poorly-differentiated gastric signet-ring cell carcinoma (SRCC) through gastroscopy in November 2020. Subsequently, she underwent laparoscopic radical gastrectomy and received a 12-cycle biweekly chemotherapy regimen of Docetaxel and Tegafur from December 2020 to January 2021. However, serum alpha-fetoprotein (AFP) concentration began to rise in September 2021, and liver tumor metastasis rapidly ensued. Given that her tumor tissue NGS revealed an amplified FGFR2 copy number of 87.1, she commenced FGFR2 inhibitor treatment in March 2022 (Fig. 3A). During the medication period, she initially received partial response (PR) and experienced a transient reduction on her liver lesion, but rapidly came to progressive disease (PD) in December 2022, manifesting multiple lesions (Fig. 3B). Similarly, serum AFP level decreased after 2 months of medication but subsequently continued to rise, reaching up to 10,000 ng/ml (Fig. 3C). As a result, we inferred that the patient initially exhibited sensitivity to FGFR2 inhibitors but swiftly developed resistance. After taking FGFR2 inhibitor for 13 months, the patient developed ascites (Fig. 3D), and pathological examination confirmed the presence of tumor cells in her ascites (Fig. 3E). To further evaluate the synergistic efficacy of dual blocking FGFR2 and SHP2 in patient-derived GC cells, we treated tumor cells derived from the patient's ascites

with AZD4547, SHP099 or their combination *in vitro* for 48 hours. Consistently, the data indicated that FGFR2 inhibitor-resistant tumor cells from her ascites were more sensitive to the combination therapy compared to AZD4547 monotherapy ($P<0.0001$) (Fig. 3F). To elucidate the underlying mechanisms, we detected the expression levels of key proteins related to FGFR2-initiated PI3K/AKT and RAS/ERK pathways after incubating tumor cells with different treatment for 1 hour. Interestingly, we didn't observe a significant downregulation of phospho-SHP2 in groups with addition of SHP099. However, combination therapy exhibited relatively stronger inhibitory effects on phospho-FGFR and its downstream molecules, including phospho-AKT and phospho-mTOR. Furthermore, the addition of SHP099 significantly suppressed phospho-ERK1/2 (Fig. 3G), suggesting that SHP099 may overcome FGFR2 inhibitor resistance mainly by suppressing RAS/ERK pathway. This case suggests that the combination of AZD4547 and SHP099 has potential application value in clinical FGFR2 inhibitor-resistant patients.

The combination of SHP099 and AZD4547 has significant anti-tumor effects in SNU-16 xenograft nude mice

To evaluate the tumor-killing capacity of combining SHP099 with AZD4547 in FGFR2-amplified GC *in vivo*, we established a subcutaneous SNU-16 xenograft model in nude mice (Fig. 4A). As anticipated, combination administration remarkably diminished tumor growth *in vivo* compared to both AZD4547 ($P<0.0001$, Fig. 4C; $P=0.0258$, Fig. 4D) and SHP099 ($P=0.0005$, Fig. 4C; $P=0.0832$, Fig. 4D) monotherapy (Fig. 4B-D and S3). Moreover, there were no notable signs of weight loss or drug toxicity observed (Fig. 4E and S4). Furthermore, consistent with *in vitro* studies, similar regulatory patterns of molecules downstream of FGFR2 were observed in protein samples derived from mouse tumor tissues. We found that combination therapy led to a more significantly suppression than single-agent treatment, especially in phospho-AKT and phospho-mTOR (Fig. 4F). To sum up, these results confirm the curative effects, elucidate the action mechanisms, and demonstrate the safety profile of combining SHP099 with AZD4547 in an *in vivo*

model.

SHP099 activates CD8$^+$ T cells and promotes its tumor-killing capacity *in vitro*

Our evidence suggested that the FGFR2-amplified group may be less likely to benefit from common immune therapies(Fuchs et al., 2018; Kim et al., 2018; Shitara et al., 2018; Wang et al., 2021). We observed that PD-L1 Combined Positive Score (CPS)-negative (CPS＜1) occurred more frequently in FGFR2-amplified GC patients compared to unamplified group in Nanjing Drum Tower Hospital cohort (Fig. 5A and S5A). Similarly, in the TCGA-STAD cohort, FGFR2-amplified GC patients exhibited lower PD-L1 mRNA expression (Fig. 5B). Meanwhile, there existed no FGFR2-amplified patients with high microsatellite instability (MSI-H) in both Nanjing Drum Tower Hospital cohort (Fig. 5A and S5B) and TCGA-STAD cohort (Fig. 5C). Furthermore, in the TCGA-STAD cohort, FGFR2-amplified GC patients showed lower Tumor Mutation Burden (TMB) levels versus unamplified group (Fig. S5C).

Considering the immunosuppressive role of SHP2 under PD-1/PD-L1 signaling, we also evaluated the effects of SHP099/AZD4547 combination therapy on T-cell immune activation *in vitro*. After incubating human PBMCs with different drug therapies for 24 hours in the presence of human anti-CD3 and anti-CD28, we observed s significant reduction of PD-1 expression in CD8$^+$ T cells in SHP099 monotherapy group (P=0.0006 vs. CD3/CD28 group) and combination therapy group (P=0.0001 vs. CD3/CD28 group) (Fig. 5D and S6A). Interestingly, we also observed a certain degree of PD-1 down-regulation in AZD4547 group (P=0.0054 vs. CD3/CD28 group) (Fig. 5D and S6A). However, only groups with the addition of SHP099 could significantly induce the production of IFN-γ in CD8$^+$ T cells (P=0.0133 SHP099 vs. CD3/CD28 group; P=0.0167 Combo vs. CD3/CD28 group) (Fig. 5E and S6B). Similarly, utilizing CBA detection, we confirmed that PBMCs treated with SHP099 monotherapy (P=0.0053 vs. CD3/CD28 group) or combined therapy (P=0.01 vs. CD3/CD28 group) secreted more IFN-γ (Fig. 5F). It’s worth noting that a notable up-regulation in CD4$^+$ T cells was also observed when incubated with combination

treatment (P＜0.0001 vs. CD3/CD28 group) (Fig. S7). Besides, T cells pre-stimulated by SHP099 monotherapy (P＜0.0001 vs. CD3/CD28 group) or combination therapy (P＜0.0001 vs. CD3/CD28 group) exhibited a more potent tumor-killing ability when incubated with FGFR2-amplified SNU-16 cells *in vitro* (Fig. 5G and H). Importantly, the cell viability of human PBMCs was not affected by drug treatment (Fig. 5I). Based on the above results, our data suggest that SHP099 may also synergize with FGFR2 inhibitor by eliciting $CD8^+$ T-cell anti-tumor immunity and improving the inhibitory TIME.

Discussion

FGFR2 amplification is a common form of genetic variations in GC, and it was identified in 5% of GC patients in TCGA-STAD cohort. Meanwhile, in our study, FGFR2 amplification occupied around 6.2% of GC patients in Nanjing Drum Tower Hospital cohort. And, it is conclusively shown that FGFR2 amplification of GC is closely related to poor prognosis. Previous study demonstrated that FGFR2 amplification was significantly associated with lymph node metastasis, poor tumor differentiation and worse survival in GC(Kim, Kim, & Jang, 2019). Consistently, FGFR2-amplifed GC patients were observed to exhibit more advanced tumor stages in our cohort. It prompted that FGFR2 amplification is a potential therapeutic target for GC.

Although FGFR2-targeted therapy has made some progress in GC treatment, there still exists problems such as low drug sensitivity and susceptibility to drug resistance. We reported a typical clinical case of a FGFR2-amplified gastric SRCC patient, showing symptoms of liver metastasis less than one year after radical gastrectomy. The patient received FGFR2 inhibitors and achieved PR after 2-month medication, with a duration of response only 7 months. This case also indicates that FGFR2-amplifed GC patients tend to have poorer prognosis and develop resistance to FGFR2 inhibitors in relative short period.

In terms of the mechanisms of FGFR2 inhibitors resistance, as early as 2013, the research in *Cancer Discovery* revealed the potential causes of FGFR2 inhibitors

resistance in FGFR3-mutated bladder cancer patients. It demonstrated that the bypass EGFR-mediated signaling activation would reduce the efficacy of FGFR inhibitors. As a result, the drug sensitivity of FGFR3-mutated bladder cancer patients to FGFR inhibitors was limited, leading to the occurrence of FGFR inhibitors resistance(Herrera-Abreu et al., 2013). Another research conducted a more in-depth exploration of this mechanism. Researchers found that in iCCA with FGFR2 fusion, feedback activation of downstream RAS/ERK, PI3K/AKT pathways mediated by EGFR alternative pathway is a significant contributor to FGFR2 inhibitors' resistance. By combining EGFR inhibitor with FGFR2 inhibitor, the feedback activation of downstream pathways was successfully relieved(Wu et al., 2022). The existing researches have recognized the crucial role played by feedback activation in RTK inhibitors resistance. And, it cannot be ruled out that there are other bypass RTK activation besides EGFR, such as HER-2, cMET, FGFR3, etc(Huang et al., 2024; Ryan et al., 2020).

SHP2 is a common molecule downstream of all RTKs. Several studied have documented that SHP2 inhibitor displayed superior anti-tumor capacity and synergistic combination efficacy with RTK inhibitors in RTK driven tumors(Chen et al., 2016; Fedele et al., 2021; Wong et al., 2018). Since SHP2 transduces signaling from all RTKs, we speculate that SHP2 inhibition can not only directly promote the anti-tumor effects of FGFR2 inhibitors, but also overcome FGFR2 inhibitors resistance by blocking all possible alternative RTK pathways. Our study first established that SHP099 can effectively promote the direct anti-tumor capacity of AZD4547 in different FGFR2-amplified GC cell lines by further suppressing downstream RAS/ERK and PI3K/AKT pathways. Meanwhile, SHP099 could continuously inhibit upstream and downstream signaling molecules and overcome FGFR2 inhibitor resistance in long-term drug stimulated tumor cells. On the contrary, AZD4547 monotherapy exhibited obvious feedback activation of downstream pathways. We also validated the combined efficacy of SHP099 and AZD4547 in a SNU-16 cell-derived xenograft (CDX) nude mouse model, and no significant drug toxicity was observed. For further research, we isolated primary tumor cells from the

FGFR2-inhibitor resistant patient's ascites. It was observed that the combination treatment with SHP099 could enhance the anti-tumor efficacy of AZD4547 by inhibiting downstream RAS/ERK and PI3K/AKT pathways. By dual blocking FGFR2 and SHP2, we successfully overcame FGFR2 inhibitors resistance by suppressing FGFR2-iniated downstream pathways in FGFR2 inhibitor-resistant patient’s cancer cells. These findings provide a potential effective approach for overcoming FGFR2 inhibitors resistance.

Previous studies only focused on drug resistance caused by bypass signaling activation of a specific RTK gene, while our study utilized SHP2 inhibitor to counteract feedback activation of downstream signaling pathways caused by all RTK activation, providing a widely applicable combination therapy model. Apart from the targeted tumor-killing capacity, we also validated the immune regulation role of SHP2 inhibition in treating FGFR2-amplified GC patients. FGFR2-amplified patients in TCGA-STAD cohort tended to have poorer PD-L1 mRNA expression and lower TMB levels compared to the unamplified group, while MSS occurred more frequently in FGFR2-amplified group. These characteristics are inextricably correlated with reduced responsiveness to anti-PD-1/PD-L1 therapy and poorer immune infiltration(Fuchs et al., 2018; Kim et al., 2018; Shitara et al., 2018; Wang et al., 2021). Meanwhile, SHP2 serves as a downstream molecule in the PD-1 signaling pathway. It has been confirmed that SHP2 can be recruited and bound to PD-1, thus inhibiting cytotoxic T cells activation by suppressing CD28 and TCR signals(Ai et al., 2020; Liu et al., 2020). Previous study has demonstrated that T-cell SHP2-deficient mice bearing colitis-associated cancer showed enhanced cytotoxicity of $CD8^+$ T cells and reduced tumor sizes(Liu et al., 2017), corroborating that SHP2 inhibition can facilitate T cell anti-tumor immunity. In addition, the combination of SHP2 inhibitor and anti-PD-1 antibody has been proved to have synergistic anti-tumor effects in colon cancer by activating cytotoxic $CD8^+$ T cells and normalizing TIME(Zhao et al., 2019). The above evidence confirmed the enormous potential value of inhibiting SHP2 in regulating anti-tumor immunity. Although several researches have revealed that SHP2 inhibitor can be ideal synergistic combination partners for various RTK inhibitors

from the perspective of targeted therapy, including MET(Pudelko et al., 2020), EGFR(Liu et al., 2021; Sun et al., 2020; Xia et al., 2021) and RET inhibitors(Lu et al., 2024), currently no in-depth study focusing on its immune regulatory function has been conducted. Our study demonstrated for the first time *in vitro* that SHP099 combing with AZD4547 down-regulated the T-cell exhaustion molecule PD-1 and up-regulated IFN-γ secretion in $CD8^+$ T cells, leading to an enhanced tumor-killing capacity of cytotoxic T lymphocytes in FGFR2-amplifed GC cell line.

Taken together, our study collectively affirmed that the combination of SHP099 and AZD4547 can not only promote the targeted tumor-killing effects and overcome AZD4547 drug resistance, but also activate T cell immunity in FGFR2-amplified GC (Fig. 6). We have validated the utility and feasibility of combining SHP2 inhibitor to FGFR2 inhibitor in FGFR2-amplified GC patients, providing an effective combination mode with both targeted intervention and immune regulation. Moreover, we also furnished sufficient evidence for the combination of RTK inhibitors and SHP2 inhibitors for all RTK-driven pan-cancer treatment.

Author contributions

J.W. and Y.W. designed the study, supervised the entire study and reviewed the manuscript. Y.Z. performed the experiments, analyzed the data and wrote the manuscript with assistance from H.W. and Y.P. Y.W. edited the pictures. X.S., T.S., J.S., L.Y. and B.L. helped to perform the experiments.

Acknowledgments

We would like to thank OrigiMed for the kind help of NGS and Nanjing University Chao Yan laboratory for the generous donation of KATOIII cell line.

Conflict of interest statement

The authors declare that they have no conflict of interest.

Ethics Statement

The study was conducted with the code of ethics of the World Medical Association (Declaration of Helsinki) and approved by the Ethics Committee of Nanjing Drum Tower Hospital (No. 2021-324-01). Human samples used in this study obtained patients' consent. All animal experiments were approved by the Institutional Animal Care and Use Committee of Drum Tower Hospital (approval number: 2022AE01029).

Reference

Ahn, S., Lee, J., Hong, M., Kim, S. T., Park, S. H., Choi, M. G.,…Kim, K. M. (2016). FGFR2 in gastric cancer: protein overexpression predicts gene amplification and high H-index predicts poor survival. *Mod Pathol*, *29*(9), 1095-1103. https://doi.org/10.1038/modpathol.2016.96

Ai, L., Xu, A., & Xu, J. (2020). Roles of PD-1/PD-L1 Pathway: Signaling, Cancer, and Beyond. *Adv Exp Med Biol*, *1248*, 33-59. https://doi.org/10.1007/978-981-15-3266-5_3

Ajani, J. A., D'Amico, T. A., Bentrem, D. J., Chao, J., Cooke, D., Corvera, C.,…Pluchino, L. A. (2022). Gastric Cancer, Version 2.2022, NCCN Clinical Practice Guidelines in Oncology. *J Natl Compr Canc Netw*, *20*(2), 167-192. https://doi.org/10.6004/jnccn.2022.0008

Babina, I. S., & Turner, N. C. (2017). Advances and challenges in targeting FGFR signalling in cancer. *Nat Rev Cancer*, *17*(5), 318-332. https://doi.org/10.1038/nrc.2017.8

Chen, Y. N., LaMarche, M. J., Chan, H. M., Fekkes, P., Garcia-Fortanet, J., Acker, M. G.,…Fortin, P. D. (2016). Allosteric inhibition of SHP2 phosphatase inhibits cancers driven by receptor tyrosine kinases. *Nature*, *535*(7610), 148-152. https://doi.org/10.1038/nature18621

Comprehensive molecular characterization of gastric adenocarcinoma. (2014). *Nature*, *513*(7517), 202-209. https://doi.org/10.1038/nature13480

Du, Z., & Lovly, C. M. (2018). Mechanisms of receptor tyrosine kinase activation in cancer. *Mol Cancer*, *17*(1), 58. https://doi.org/10.1186/s12943-018-0782-4

Fedele, C., Li, S., Teng, K. W., Foster, C. J. R., Peng, D., Ran, H.,…Neel, B. G. (2021). SHP2 inhibition diminishes KRASG12C cycling and promotes tumor microenvironment remodeling. *J Exp Med*, *218*(1). https://doi.org/10.1084/jem.20201414

Fuchs, C. S., Doi, T., Jang, R. W., Muro, K., Satoh, T., Machado, M.,…Yoon, H. H. (2018). Safety and Efficacy of Pembrolizumab Monotherapy in Patients With Previously Treated Advanced Gastric and Gastroesophageal Junction Cancer: Phase 2 Clinical KEYNOTE-059 Trial. *JAMA Oncol*, *4*(5), e180013. https://doi.org/10.1001/jamaoncol.2018.0013

Gordon, A., Johnston, E., Lau, D. K., & Starling, N. (2022). Targeting FGFR2 Positive Gastroesophageal Cancer: Current and Clinical Developments. *Onco Targets Ther*, *15*, 1183-1196. https://doi.org/10.2147/ott.S282718

Guan, W. L., He, Y., & Xu, R. H. (2023). Gastric cancer treatment: recent progress and future perspectives. *J Hematol Oncol*, *16*(1), 57. https://doi.org/10.1186/s13045-023-01451-3

Herrera-Abreu, M. T., Pearson, A., Campbell, J., Shnyder, S. D., Knowles, M. A., Ashworth, A., & Turner, N. C. (2013). Parallel RNA interference screens identify EGFR activation as an escape mechanism in FGFR3-mutant cancer. *Cancer Discov*, *3*(9), 1058-1071. https://doi.org/10.1158/2159-8290.Cd-12-0569

Huang, P., Ji, F., Cheung, A. H., Fu, K., Zhou, Q., Ding, X.,…Wong, C. C. (2024). Peptostreptococcus stomatis promotes colonic tumorigenesis and receptor tyrosine kinase inhibitor resistance by activating ERBB2-MAPK. *Cell Host Microbe*. https://doi.org/10.1016/j.chom.2024.07.001

Hur, J. Y., Chao, J., Kim, K., Kim, S. T., Kim, K. M., Klempner, S. J., & Lee, J. (2020). High-level FGFR2 amplification is associated with poor prognosis and Lower response to chemotherapy in gastric cancers. *Pathol Res Pract*, *216*(4), 152878. https://doi.org/10.1016/j.prp.2020.152878

Janjigian, Y. Y., Shitara, K., Moehler, M., Garrido, M., Salman, P., Shen, L.,…Ajani, J. A. (2021). First-line nivolumab plus chemotherapy versus chemotherapy alone for advanced gastric, gastro-oesophageal junction, and oesophageal adenocarcinoma (CheckMate 649): a randomised, open-label, phase 3 trial. *Lancet*, *398*(10294), 27-40. https://doi.org/10.1016/s0140-6736(21)00797-2

Jogo, T., Nakamura, Y., Shitara, K., Bando, H., Yasui, H., Esaki, T.,…Yoshino, T. (2021). Circulating Tumor DNA Analysis Detects FGFR2 Amplification and Concurrent Genomic Alterations Associated with FGFR Inhibitor Efficacy in Advanced Gastric Cancer. *Clin Cancer Res*, *27*(20), 5619-5627. https://doi.org/10.1158/1078-0432.Ccr-21-1414

Kang, C. (2023). Trastuzumab Deruxtecan: A Review in Gastric or Gastro-Oesophageal Junction Adenocarcinoma. *Target Oncol*, *18*(6), 981-989. https://doi.org/10.1007/s11523-023-00998-y

Katoh, M., Loriot, Y., Brandi, G., Tavolari, S., Wainberg, Z. A., & Katoh, M. (2024). FGFR-targeted therapeutics: clinical activity, mechanisms of resistance and new directions. *Nat Rev Clin Oncol*, *21*(4), 312-329. https://doi.org/10.1038/s41571-024-00869-z

Katoh, M., & Nakagama, H. (2014). FGF receptors: cancer biology and therapeutics. *Med Res Rev*, *34*(2), 280-300. https://doi.org/10.1002/med.21288

Kim, H. S., Kim, J. H., & Jang, H. J. (2019). Pathologic and prognostic impacts of FGFR2 amplification in gastric cancer: a meta-analysis and systemic review. *J Cancer*, *10*(11), 2560-2567. https://doi.org/10.7150/jca.29184

Kim, H. S., Kim, J. H., Jang, H. J., Han, B., & Zang, D. Y. (2019). Pathological and Prognostic Impacts of FGFR2 Overexpression in Gastric Cancer: A Meta-Analysis. *J Cancer*, *10*(1), 20-27. https://doi.org/10.7150/jca.28204

Kim, S. T., Cristescu, R., Bass, A. J., Kim, K. M., Odegaard, J. I., Kim, K.,…Kang, W. K. (2018). Comprehensive molecular characterization of clinical responses to PD-1 inhibition in metastatic gastric cancer. *Nat Med*, *24*(9), 1449-1458. https://doi.org/10.1038/s41591-018-0101-z

Koh, J., Nam, S. K., Roh, H., Kim, J., Lee, B. C., Kim, J. W.,…Lee, H. S. (2019). Somatic mutational profiles of stage II and III gastric cancer according to tumor microenvironment immune type. *Genes Chromosomes Cancer*, *58*(1), 12-22. https://doi.org/10.1002/gcc.22683

Lee, S., Rauch, J., & Kolch, W. (2020). Targeting MAPK Signaling in Cancer: Mechanisms of Drug Resistance and Sensitivity. *Int J Mol Sci*, *21*(3). https://doi.org/10.3390/ijms21031102

Li, J., Jie, H. B., Lei, Y., Gildener-Leapman, N., Trivedi, S., Green, T.,…Ferris, R. L. (2015). PD-1/SHP-2 inhibits Tc1/Th1 phenotypic responses and the activation of T cells in the tumor microenvironment. *Cancer Res*, *75*(3), 508-518. https://doi.org/10.1158/0008-5472.Can-14-1215

Liu, C., Lu, H., Wang, H., Loo, A., Zhang, X., Yang, G.,…Hao, H. X. (2021). Combinations with Allosteric SHP2 Inhibitor TNO155 to Block Receptor Tyrosine Kinase Signaling. *Clin Cancer Res*, *27*(1), 342-354. https://doi.org/10.1158/1078-0432.Ccr-20-2718

Liu, Q., Qu, J., Zhao, M., Xu, Q., & Sun, Y. (2020). Targeting SHP2 as a promising strategy for cancer immunotherapy. *Pharmacol Res*, *152*, 104595. https://doi.org/10.1016/j.phrs.2019.104595

Liu, W., Guo, W., Shen, L., Chen, Z., Luo, Q., Luo, X.,…Sun, Y. (2017). T lymphocyte SHP2-deficiency triggers anti-tumor immunity to inhibit colitis-associated cancer in mice. *Oncotarget*, *8*(5), 7586-7597. https://doi.org/10.18632/oncotarget.13812

Lu, X., Yu, R., Li, Z., Yang, M., Dai, J., & Liu, M. (2024). JC-010a, a novel selective SHP2 allosteric inhibitor, overcomes RTK/non-RTK-mediated drug resistance in multiple oncogene-addicted cancers. *Cancer Lett*, *582*, 216517. https://doi.org/10.1016/j.canlet.2023.216517

Paul, M. D., & Hristova, K. (2019). The RTK Interactome: Overview and Perspective on RTK Heterointeractions. *Chem Rev*, *119*(9), 5881-5921. https://doi.org/10.1021/acs.chemrev.8b00467

Pearson, A., Smyth, E., Babina, I. S., Herrera-Abreu, M. T., Tarazona, N., Peckitt, C.,…Turner, N. C. (2016). High-Level Clonal FGFR Amplification and Response to FGFR Inhibition in a Translational Clinical Trial. *Cancer Discov*, *6*(8), 838-851. https://doi.org/10.1158/2159-8290.Cd-15-1246

Pudelko, L., Jaehrling, F., Reusch, C., Vitri, S., Stroh, C., Linde, N.,…Karachaliou, N. (2020). SHP2 Inhibition Influences Therapeutic Response to Tepotinib in Tumors with MET Alterations. *iScience*, *23*(12), 101832. https://doi.org/10.1016/j.isci.2020.101832

Ryan, M. B., Fece de la Cruz, F., Phat, S., Myers, D. T., Wong, E., Shahzade, H. A.,…Corcoran, R. B. (2020). Vertical Pathway Inhibition Overcomes Adaptive Feedback Resistance to KRAS(G12C) Inhibition. *Clin Cancer Res*, *26*(7), 1633-1643. https://doi.org/10.1158/1078-0432.Ccr-19-3523

Shitara, K., Özgüroğlu, M., Bang, Y. J., Di Bartolomeo, M., Mandalà, M., Ryu, M. H.,…Fuchs, C. S. (2018). Pembrolizumab versus paclitaxel for previously treated, advanced gastric or gastro-oesophageal junction cancer (KEYNOTE-061): a randomised, open-label, controlled, phase 3 trial. *Lancet*, *392*(10142), 123-133. https://doi.org/10.1016/s0140-6736(18)31257-1

Smyth, E. C., Nilsson, M., Grabsch, H. I., van Grieken, N. C., & Lordick, F. (2020). Gastric cancer. *Lancet*, *396*(10251), 635-648. https://doi.org/10.1016/s0140-6736(20)31288-5

Sodir, N. M., Pathria, G., Adamkewicz, J. I., Kelley, E. H., Sudhamsu, J., Merchant, M.,…Maddalo, D. (2023). SHP2: A Pleiotropic Target at the Interface of

Cancer and Its Microenvironment. *Cancer Discov*, *13*(11), 2339-2355. https://doi.org/10.1158/2159-8290.Cd-23-0383

Song, Y., Zhao, M., Zhang, H., & Yu, B. (2022). Double-edged roles of protein tyrosine phosphatase SHP2 in cancer and its inhibitors in clinical trials. *Pharmacol Ther*, *230*, 107966. https://doi.org/10.1016/j.pharmthera.2021.107966

Song, Z., Wu, Y., Yang, J., Yang, D., & Fang, X. (2017). Progress in the treatment of advanced gastric cancer. *Tumour Biol*, *39*(7), 1010428317714626. https://doi.org/10.1177/1010428317714626

Sun, Y., Meyers, B. A., Czako, B., Leonard, P., Mseeh, F., Harris, A. L.,…Jones, P. (2020). Allosteric SHP2 Inhibitor, IACS-13909, Overcomes EGFR-Dependent and EGFR-Independent Resistance Mechanisms toward Osimertinib. *Cancer Res*, *80*(21), 4840-4853. https://doi.org/10.1158/0008-5472.Can-20-1634

Van Cutsem, E., Bang, Y. J., Mansoor, W., Petty, R. D., Chao, Y., Cunningham, D.,…Landers, D. (2017). A randomized, open-label study of the efficacy and safety of AZD4547 monotherapy versus paclitaxel for the treatment of advanced gastric adenocarcinoma with FGFR2 polysomy or gene amplification. *Ann Oncol*, *28*(6), 1316-1324. https://doi.org/10.1093/annonc/mdx107

Wainberg, Z. A., Enzinger, P. C., Kang, Y. K., Qin, S., Yamaguchi, K., Kim, I. H.,…Lee, K. W. (2022). Bemarituzumab in patients with FGFR2b-selected gastric or gastro-oesophageal junction adenocarcinoma (FIGHT): a randomised, double-blind, placebo-controlled, phase 2 study. *Lancet Oncol*, *23*(11), 1430-1440. https://doi.org/10.1016/s1470-2045(22)00603-9

Wang, D., Wang, N., Li, X., Chen, X., Shen, B., Zhu, D.,…Shu, Y. (2021). Tumor mutation burden as a biomarker in resected gastric cancer via its association with immune infiltration and hypoxia. *Gastric Cancer*, *24*(4), 823-834. https://doi.org/10.1007/s10120-021-01175-8

Wei, L., Sun, J., Zhang, N., Zheng, Y., Wang, X., Lv, L.,…Yang, M. (2020). Noncoding RNAs in gastric cancer: implications for drug resistance. *Mol Cancer*, *19*(1), 62. https://doi.org/10.1186/s12943-020-01185-7

Wong, G. S., Zhou, J., Liu, J. B., Wu, Z., Xu, X., Li, T.,…Bass, A. J. (2018). Targeting wild-type KRAS-amplified gastroesophageal cancer through combined MEK and SHP2 inhibition. *Nat Med*, *24*(7), 968-977. https://doi.org/10.1038/s41591-018-0022-x

Wu, Q., Zhen, Y., Shi, L., Vu, P., Greninger, P., Adil, R.,…Bardeesy, N. (2022). EGFR Inhibition Potentiates FGFR Inhibitor Therapy and Overcomes Resistance in FGFR2 Fusion-Positive Cholangiocarcinoma. *Cancer Discov*, *12*(5), 1378-1395. https://doi.org/10.1158/2159-8290.Cd-21-1168

Xia, L., Yang, F., Wu, X., Li, S., Kan, C., Zheng, H., & Wang, S. (2021). SHP2 inhibition enhances the anticancer effect of Osimertinib in EGFR T790M mutant lung adenocarcinoma by blocking CXCL8 loop mediated stemness. *Cancer Cell Int*, *21*(1), 337. https://doi.org/10.1186/s12935-021-02056-x

Xie, L., Su, X., Zhang, L., Yin, X., Tang, L., Zhang, X.,…Ji, Q. (2013). FGFR2 gene amplification in gastric cancer predicts sensitivity to the selective FGFR inhibitor AZD4547. *Clin Cancer Res*, *19*(9), 2572-2583. https://doi.org/10.1158/1078-0432.Ccr-12-3898

Yang, Y. M., Hong, P., Xu, W. W., He, Q. Y., & Li, B. (2020). Advances in targeted therapy for esophageal cancer. *Signal Transduct Target Ther*, *5*(1), 229. https://doi.org/10.1038/s41392-020-00323-3

Zhao, J. J., Yap, D. W. T., Chan, Y. H., Tan, B. K. J., Teo, C. B., Syn, N. L.,…Sundar, R. (2022). Low Programmed Death-Ligand 1-Expressing Subgroup Outcomes of First-Line Immune Checkpoint Inhibitors in Gastric or Esophageal Adenocarcinoma. *J Clin Oncol*, *40*(4), 392-402. https://doi.org/10.1200/jco.21.01862

Zhao, M., Guo, W., Wu, Y., Yang, C., Zhong, L., Deng, G.,…Sun, Y. (2019). SHP2 inhibition triggers anti-tumor immunity and synergizes with PD-1 blockade. *Acta Pharm Sin B*, *9*(2), 304-315. https://doi.org/10.1016/j.apsb.2018.08.009

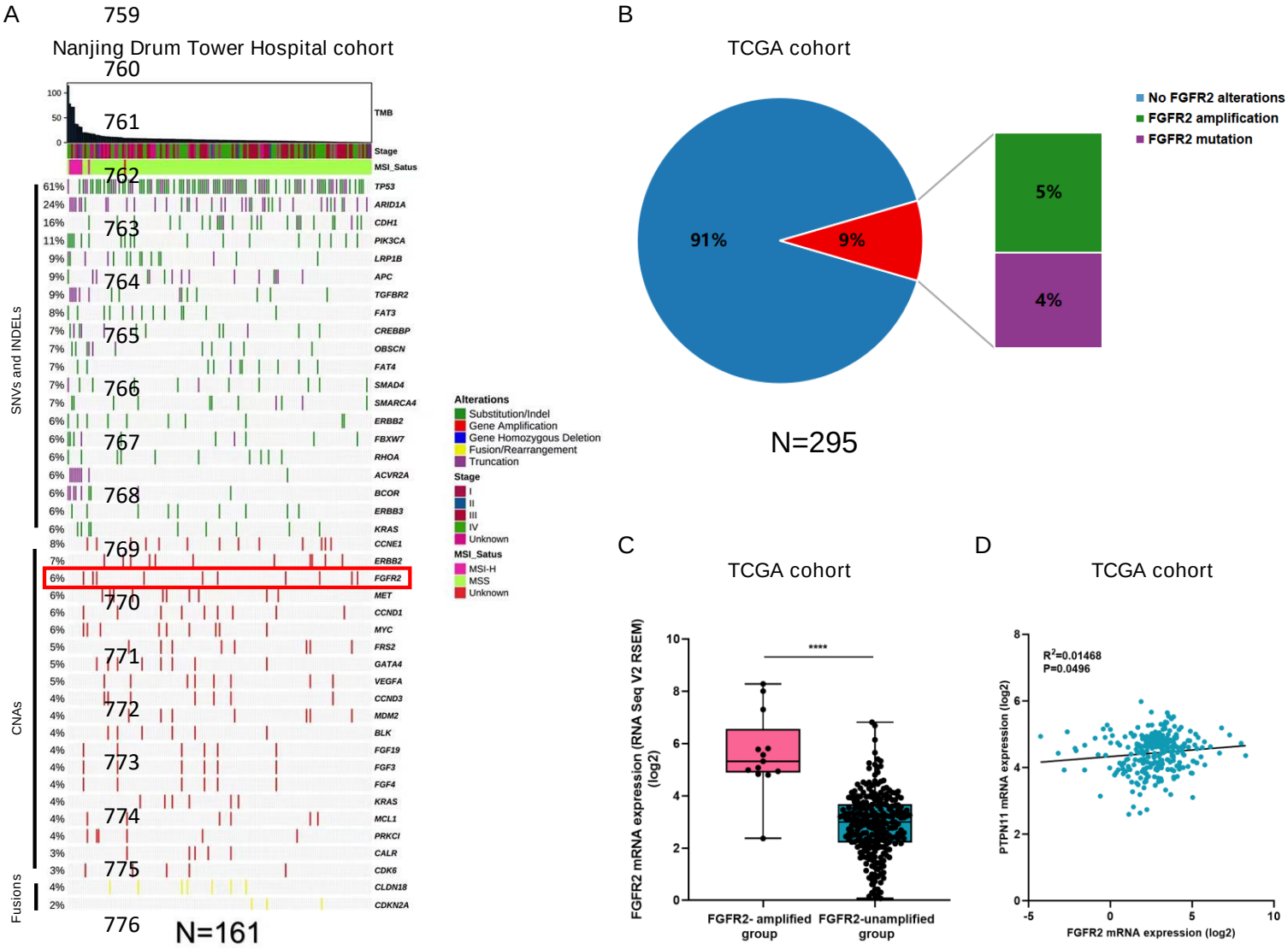
A
Nanjing Drum Tower Hospital cohort
TMB
Stage
MSI_Satus
SNVs and INDELs
CNAs
Fusions
TP53
ARID1A
CDH1
PIK3CA
LRP1B
APC
TGFBR2
FAT3
CREBBP
OBSCN
FAT4
SMAD4
SMARCA4
ERBB2
FBXW7
RHOA
ACVR2A
BCOR
ERBB3
KRAS
CCNE1
ERBB2
FGFR2
MET
CCND1
MYC
FRS2
GATA4
VEGFA
CCND3
MDM2
BLK
FGF19
FGF3
FGF4
KRAS
MCL1
PRKCI
CALR
CDK6
CLDN18
CDKN2A
N=161
Alterations
Substitution/Indel
Gene Amplification
Gene Homozygous Deletion
Fusion/Rearrangement
Truncation
Stage
I
II
III
IV
Unknown
MSI_Satus
MSI-H
MSS
Unknown
B
TCGA cohort
No FGFR2 alterations
FGFR2 amplification
FGFR2 mutation
91%
9%
5%
4%
N=295
C
TCGA cohort
FGFR2 mRNA expression (RNA Seq V2 RSEM) (log2)
****
FGFR2- amplified group
FGFR2-unamplified group
D
TCGA cohort
R2=0.01468
P=0.0496
PTPN11 mRNA expression (log2)
FGFR2 mRNA expression (log2)

Fig 1. Recurrent FGFR2 gene amplification in Chinese GC patients. (A) Overview of genomic alterations in GC patient samples collected in Nanjing Drum Tower Hospital (n=161). The patient samples are shown on the x-axis. Information of TMB, stage, MSI-status and significantly altered genes are shown on the y-axis, with frequency of each alteration annotated on the left of the waterfall plot. **(B)** Pie chart displaying the proportion of FGFR2 alterations in TCGA STAD cohort (n=295). **(C)** FGFR2 mRNA expression levels were analyzed between FGFR2-amplified group (n=13) and FGFR2-unamplified group (n=250) from TCGA-STAD cohort. **(D)** Correlation between PTPN11 and FGFR2 mRNA expressions among samples from TCGA-STAD hohort. Data are shown as Mean±SEM. ****$p < 0.0001$. P values are detemined by unpaired t test or linear regression t test.

A

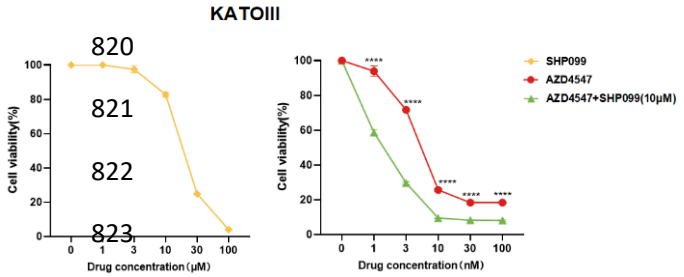
KATOIII
Cell viability(%)
Drug concentration (μM)
Drug concentration (nM)
SHP099
AZD4547
AZD4547+SHP099(10μM)

B

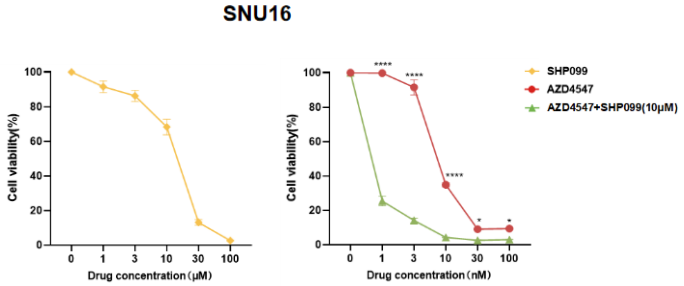
SNU16
Cell viability(%)
Drug concentration (μM)
Drug concentration (nM)
SHP099
AZD4547
AZD4547+SHP099(10μM)

C

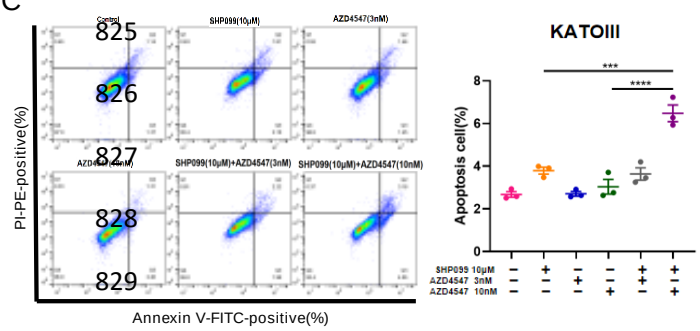
PI-PE-positive(%)
Annexin V-FITC-positive(%)
KATOIII
Apoptosis cell(%)
SHP099 10μM
AZD4547 3nM
AZD4547 10nM

D

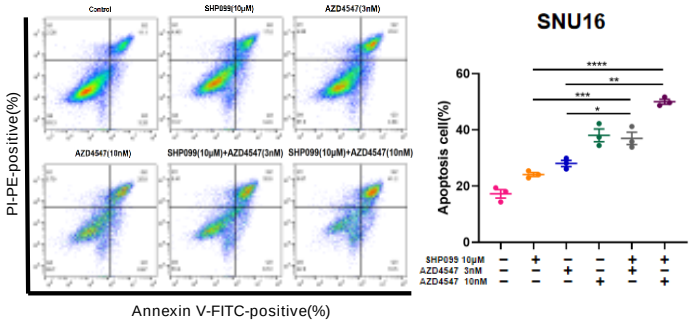
PI-PE-positive(%)
Annexin V-FITC-positive(%)
SNU16
Apoptosis cell(%)
SHP099 10μM
AZD4547 3nM
AZD4547 10nM

E

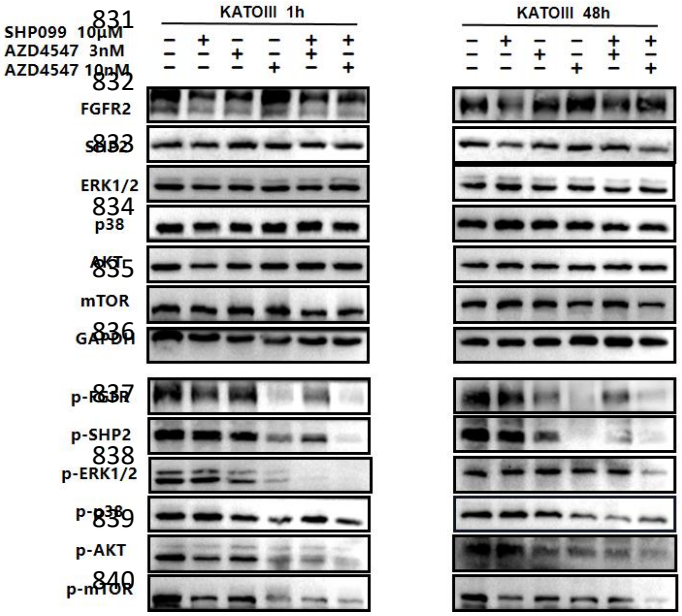
KATOIII 1h
KATOIII 48h
SHP099 10μM
AZD4547 3nM
AZD4547 10nM
FGFR2
SHP2
ERK1/2
p38
AKT
mTOR
GAPDH
p-FGFR
p-SHP2
p-ERK1/2
p-p38
p-AKT
p-mTOR

F

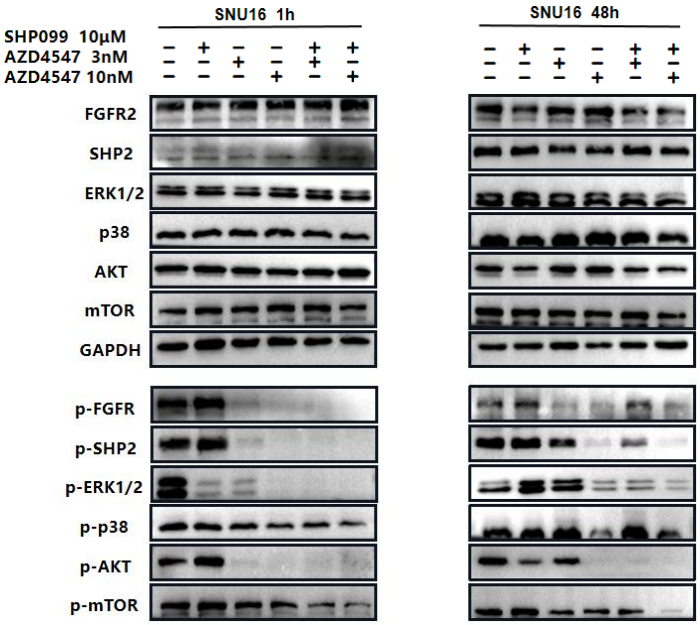
SNU16 1h
SNU16 48h
SHP099 10μM
AZD4547 3nM
AZD4547 10nM
FGFR2
SHP2
ERK1/2
p38
AKT
mTOR
GAPDH
p-FGFR
p-SHP2
p-ERK1/2
p-p38
p-AKT
p-mTOR

Fig 2. SHP099 enhances the antitumor effects and overcomes the resistance of FGFR2 inhibitors in FGFR2-amplified GC. Sensitivity of **(A)** KATOIII and **(B)** SNU-16 to SHP099, AZD4547 or combination therapy with different concentration gradients. Effects of different treatments on cell apoptosis of **(C)** KATOIII and **(D)** SNU-16 after 48-hour drugs incubation. **(E)** KATOIII and **(F)** SNU-16 were incubated with vehicle, SHP099 10 μM, AZD4547 3nM or combination therapies for 1 hour or 48 hours, then cell lysates were immunoblotted for phospho-FGFR and total-FGFR2, phospho-SHP2 and total-SHP2, phospho-Erk and total-Erk, phospho-p38 and total-p38, phospho-AKT and total-AKT, and phospho-mTOR and total-mTOR. Data are shown as Mean±SEM. *$p < 0.05$, **$p < 0.01$, ***$p < 0.001$, ****$p < 0.0001$. P values are detemined by ordinary one-way ANOVA or two-way ANOVA.

A

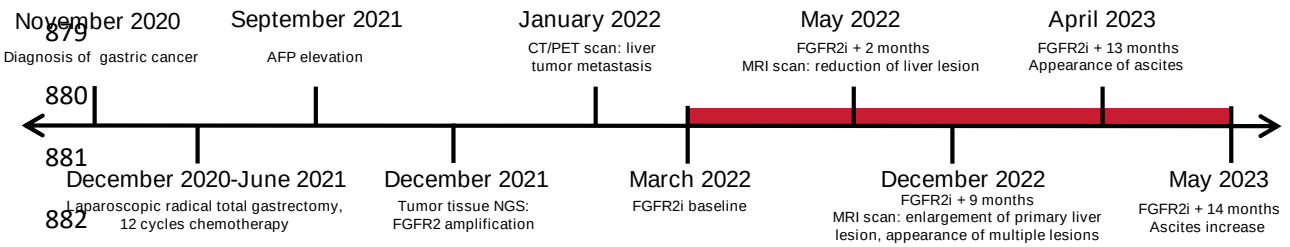
November 2020
Diagnosis of gastric cancer
September 2021
AFP elevation
January 2022
CT/PET scan: liver tumor metastasis
May 2022
FGFR2i + 2 months
MRI scan: reduction of liver lesion
April 2023
FGFR2i + 13 months
Appearance of ascites
December 2020-June 2021
Laparoscopic radical total gastrectomy, 12 cycles chemotherapy
December 2021
Tumor tissue NGS: FGFR2 amplification
March 2022
FGFR2i baseline
December 2022
FGFR2i + 9 months
MRI scan: enlargement of primary liver lesion, appearance of multiple lesions
May 2023
FGFR2i + 14 months
Ascites increase

B

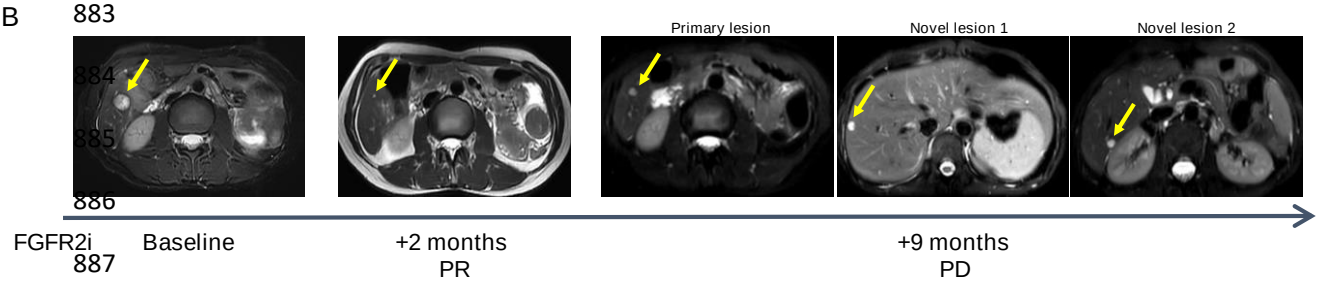
Primary lesion
Novel lesion 1
Novel lesion 2
FGFR2i
Baseline
+2 months
PR
+9 months
PD

C

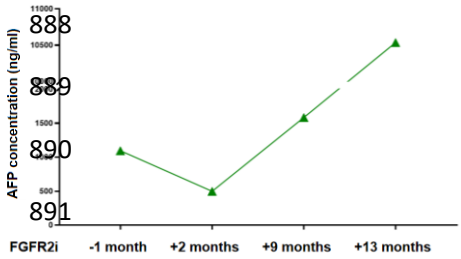
AFP concentration (ng/ml)
FGFR2i
-1 month
+2 months
+9 months
+13 months

D

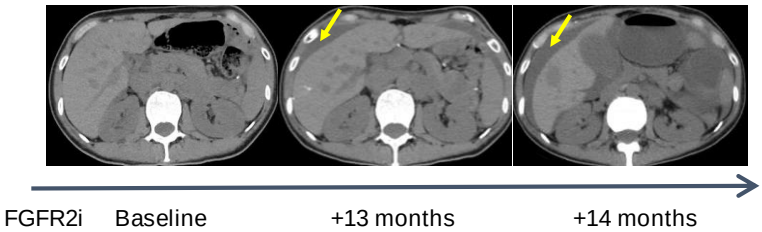
FGFR2i
Baseline
+13 months
+14 months

E

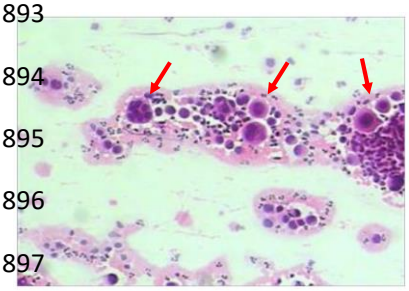

F

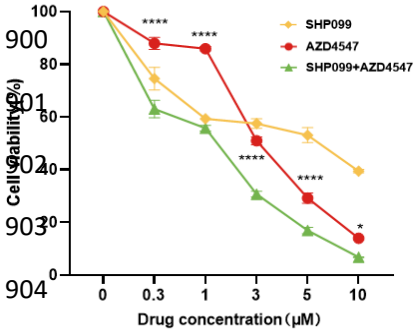
SHP099
AZD4547
SHP099+AZD4547
Cell Viability(%)
Drug concentration (μM)

G

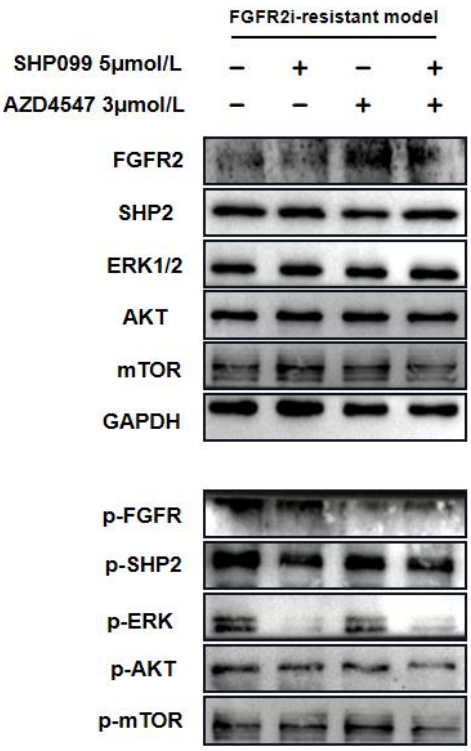
FGFR2i-resistant model
SHP099 5μmol/L
AZD4547 3μmol/L
FGFR2
SHP2
ERK1/2
AKT
mTOR
GAPDH
p-FGFR
p-SHP2
p-ERK
p-AKT
p-mTOR

Fig 3. The synergistic efficacy of combining AZD4547 with SHP099 in primary tumor cells derived from a FGFR2 inhibitor-resistant GC patient. (A) Schematic of therapeutic process of the FGFR2-amplified GC patient who was previously sensitive to FGFR2 inhibitors but quickly became resistant. **(B)** Representative CT and MRI images of recurrent liver lesions at different time points. Liver lesions are indicated by yellow arrows. **(C)** Representive CT images displaying the occurrence and progression of ascites. Ascites are indicatied by yellow arrows. **(D)** Pathology of malignant asites from this FGFR2 inhibitor-resistant patient. Tumor cells are indicated by red arrows. **(E)** AFP concentration variations of the patient during FGFR2 inhibitors medication. **(F)** Sensitivity of cancer cells from FGFR2 inhibitor-resistant patient's asites to FGFR2 inhibitor AZD4547, SHP2 inhibitor SHP099 or combined administration with different concentration gradients. Data are shown as Mean±SEM. *$p < 0.05$, ****$p < 0.0001$. P values are detemined by two-way ANOVA. **(G)** Tumor cells from asites were incubated with vehicle, SHP099 5 μM, AZD4547 3 μM or combination therapy for 1 hour, then cell lysates were immunoblotted for phospho-FGFR and total-FGFR2, phospho-SHP2 and total-SHP2, phospho-Erk and total-Erk, phospho-AKT and total-AKT, and phospho-mTOR and total-mTOR.

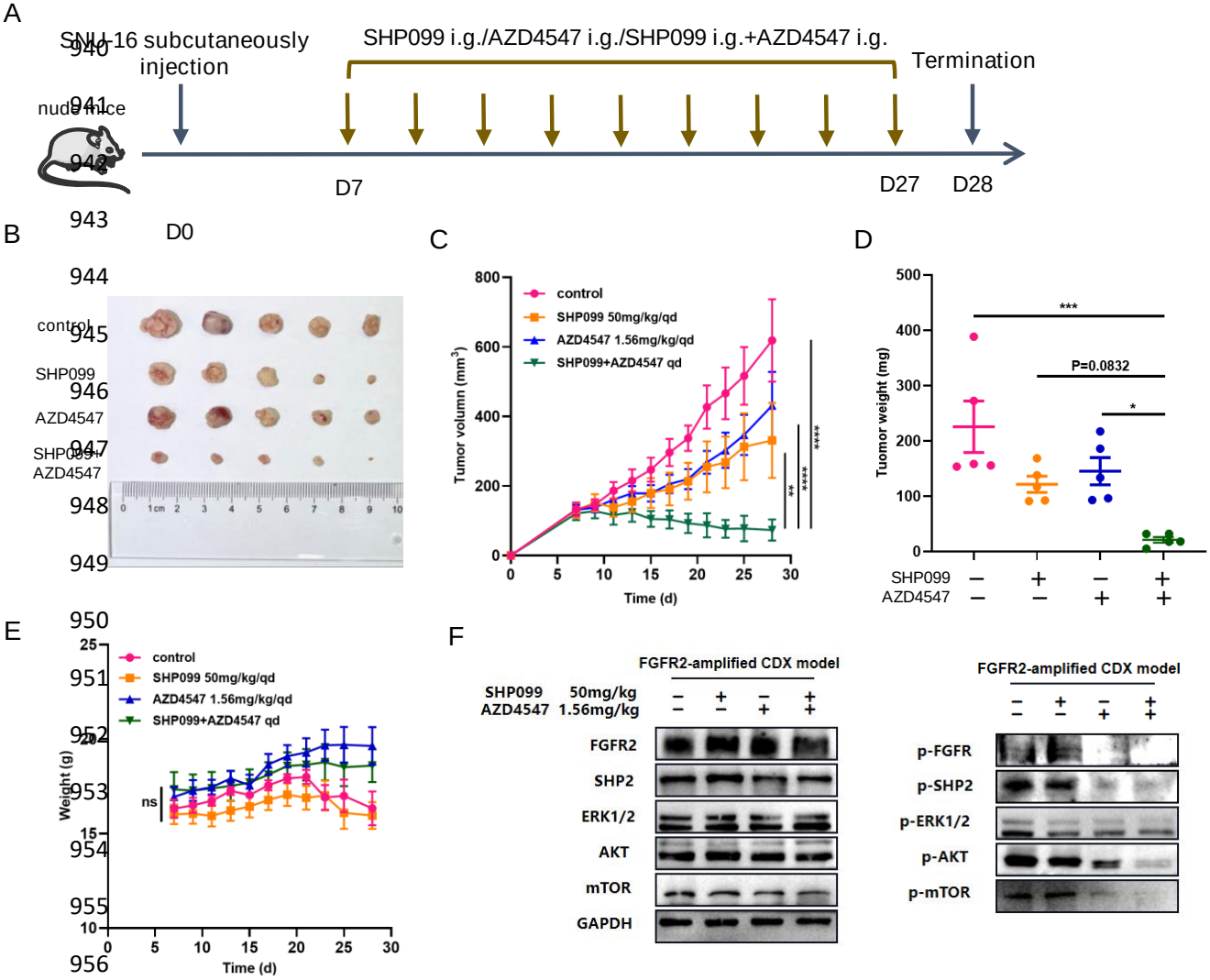
A
SNU-16 subcutaneously injection
SHP099 i.g./AZD4547 i.g./SHP099 i.g.+AZD4547 i.g.
Termination
nude mice
D0
D7
D27
D28
B
control
SHP099
AZD4547
SHP099+ AZD4547
C
control
SHP099 50mg/kg/qd
AZD4547 1.56mg/kg/qd
SHP099+AZD4547 qd
Tumor volumn (mm³)
Time (d)
D
Tuomor weight (mg)
P=0.0832
SHP099
AZD4547
E
Weight (g)
ns
Time (d)
F
FGFR2-amplified CDX model
SHP099 50mg/kg
AZD4547 1.56mg/kg
FGFR2
SHP2
ERK1/2
AKT
mTOR
GAPDH
p-FGFR
p-SHP2
p-ERK1/2
p-AKT
p-mTOR

Fig 4. The combination of SHP099 and AZD4547 has significant anti-tumor effects in SNU-16 xenograft nude mice. BALB/c nude mice were injected with 1×10^7 SNU-16 cancer cells and received different formulations by oral gavage every day upon tumor volumes reached 100-150 mm^3. **(A)** Schematic of SHP099 and AZD4547 therapeutic schedule in FGFR2-amplified SNU-16 subcutaneous xenograft model. **(B)** Body weights, **(C)** tumor volumes and **(D)** tumor weights of different groups. **(E)** Representative images of tumors. **(F)** Tumors were harvested 6 hours after the last dose of drugs, and cell lysates from tumor tissues were immunoblotted for phospho-FGFR and total-FGFR2, phospho-SHP2 and total-SHP2, phospho-Erk and total-Erk, phospho-AKT and total-AKT, and phospho-mTOR and total-mTOR. Data are shown as Mean±SEM. ns, not significant, $*p < 0.05$, $**p < 0.01$, $***p < 0.001$, $****p < 0.0001$. P values are detemined by ordinary one-way ANOVA or two-way ANOVA.

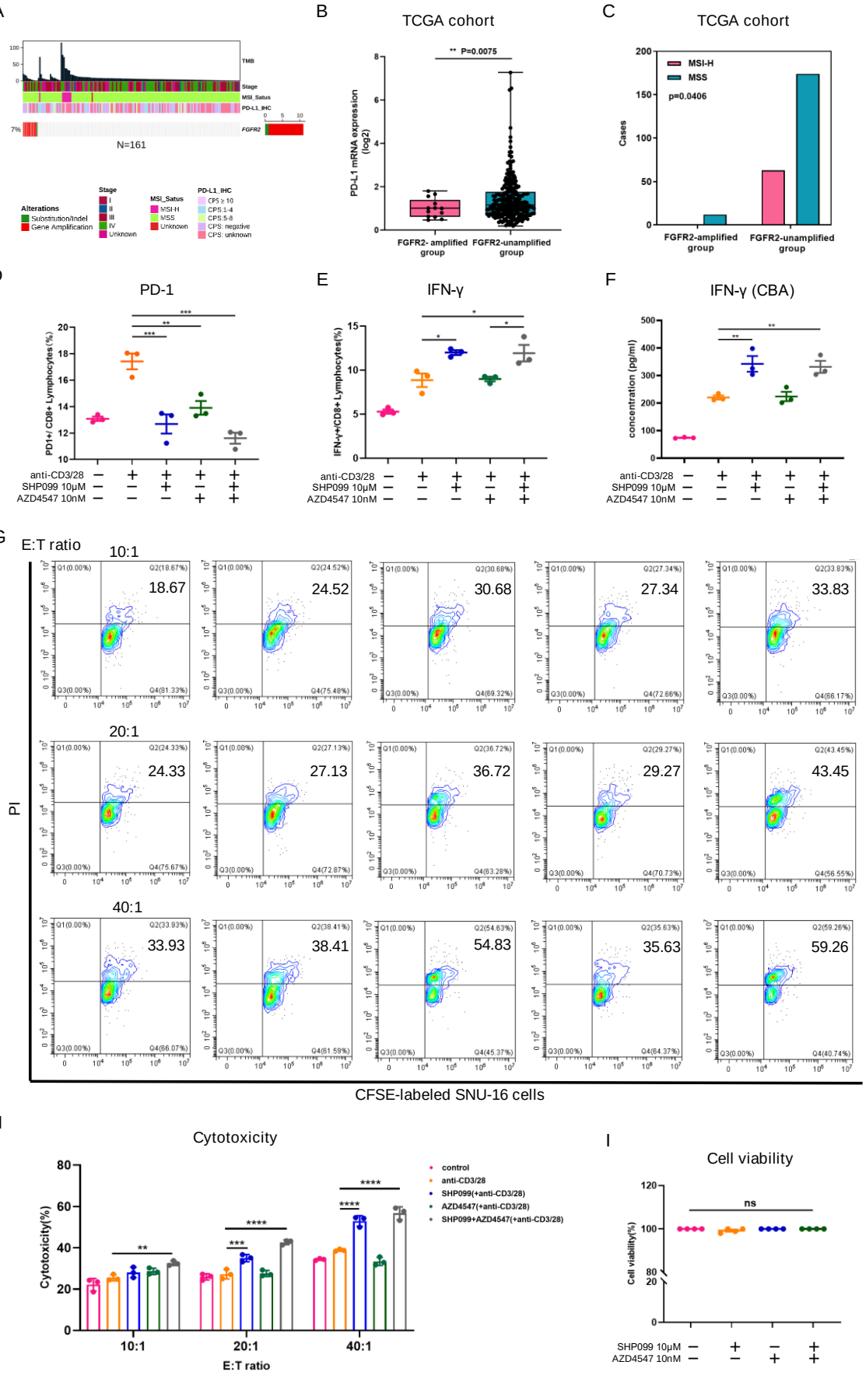
A
TMB
Stage
MSI_Satus
PD-L1_IHC
FGFR2
N=161
Alterations
Substitution/Indel
Gene Amplification
Stage
I
II
III
IV
Unknown
MSI_Satus
MSI-H
MSS
Unknown
PD-L1_IHC
CPS ≥ 10
CPS:1-4
CPS:5-8
CPS: negative
CPS: unknown
B
TCGA cohort
** P=0.0075
PD-L1 mRNA expression (log2)
FGFR2- amplified group
FGFR2-unamplified group
C
TCGA cohort
MSI-H
MSS
p=0.0406
Cases
FGFR2-amplified group
FGFR2-unamplified group
D
PD-1
PD1+/ CD8+ Lymphocytes(%)
anti-CD3/28
SHP099 10μM
AZD4547 10nM
E
IFN-γ
IFN-γ+/CD8+ Lymphocytes(%)
anti-CD3/28
SHP099 10μM
AZD4547 10nM
F
IFN-γ (CBA)
concentration (pg/ml)
anti-CD3/28
SHP099 10μM
AZD4547 10nM
G
E:T ratio
10:1
18.67
24.52
30.68
27.34
33.83
20:1
24.33
27.13
36.72
29.27
43.45
40:1
33.93
38.41
54.83
35.63
59.26
PI
CFSE-labeled SNU-16 cells
H
Cytotoxicity
Cytotoxicity(%)
control
anti-CD3/28
SHP099(+anti-CD3/28)
AZD4547(+anti-CD3/28)
SHP099+AZD4547(+anti-CD3/28)
10:1
20:1
40:1
E:T ratio
I
Cell viability
ns
Cell viability(%)
SHP099 10μM
AZD4547 10nM

Fig 5. SHP099 activates CD8+ T cells and promotes its tumor-killing capacity in vitro. (A) Overview of FGFR2 alterations individually in GC patients from Nanjing Drum Tower hospital cohort. **(B)** PD-L1 mRNA expression levels were analyzed between FGFR2-amplified group (n=13) and FGFR2-unamplified group (n=250) from TCGA-STAD cohort. **(C)** Proportions of MSI-H or MSS in FGFR2-amplified group (n=12) and FGFR2-unamplified group (n=237) from TCGA-STAD cohort. Human peripheral blood mononuclear cells (PBMCs) were incubated with different administrations in the presence of 0.25 μg/ml human anti-CD3 and 1 μg/ml human anti-CD28. Proportions of **(D)** PD-1+/CD8+ cells and **(E)** IFN-γ/CD8+ cells were detected by flow cytometry assay after 24-hour of drugs incubation. **(F)** Expression levels of IFN-γ in cellular supernatant were measured by Cytometric Bead Array (CBA) assay after 24-hour of drugs incubation. **(G, H)** After 48-hour of advance drugs stimulation in human PBMCs, cytotoxicities of human PBMCs against SNU-16 at different E:T ratios of 10:1, 20:1, 40:1 were analyzed by flow cytometry assay after CFSE/PI staining. **(I)** Cell viability of human PBMCs after 48-hour of drugs incubation. Data are shown as Mean±SEM. ns, not significant, *$p < 0.05$, **$p < 0.01$, ***$p < 0.001$, ****$p < 0.0001$. P values are detemined by Welch's t test, Fisher's exact test, ordinary one-way ANOVA or two-way ANOVA.

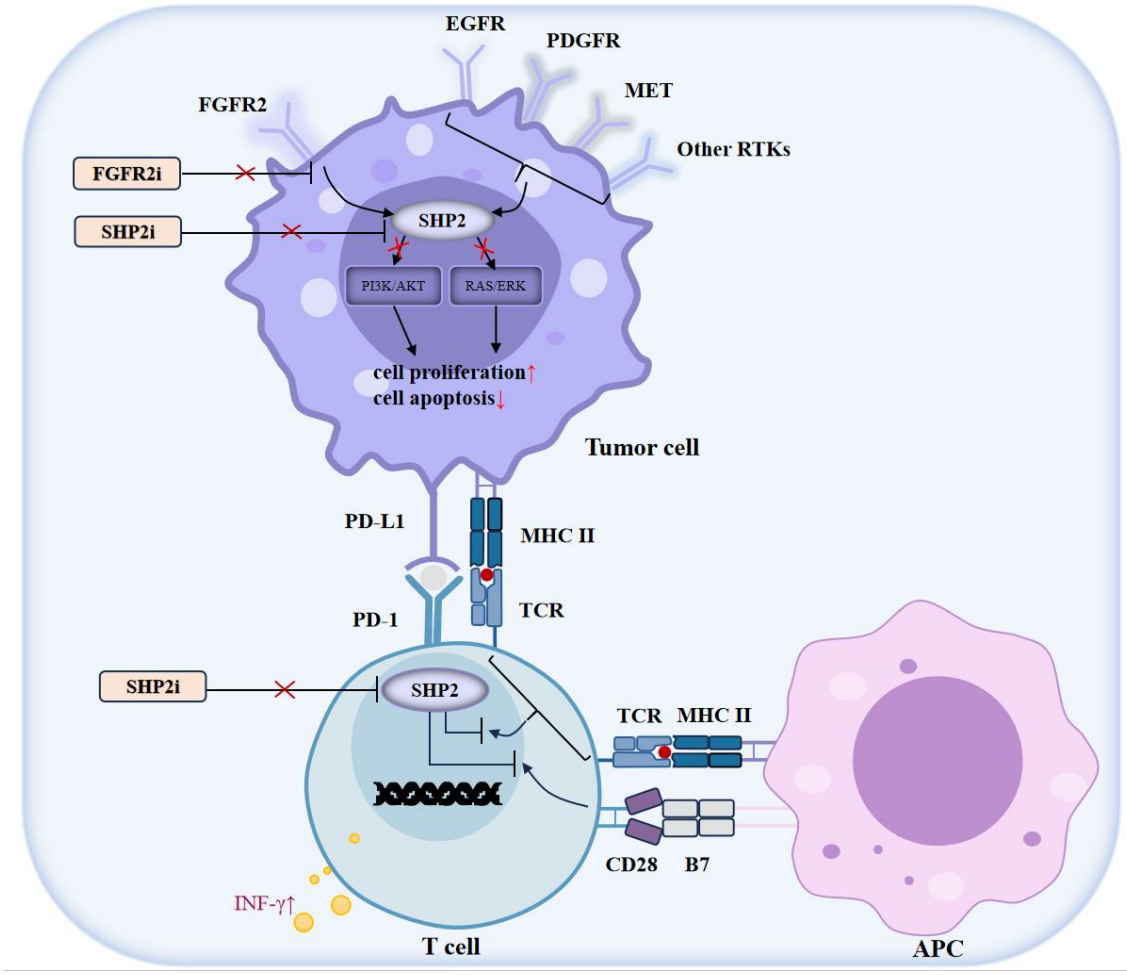

Fig 6. Schematic of the mechasims of blocking SHP2 and FGFR2 in inhibiting tumor progression by targeted therapy and immune intervention. On one hand, SHP2 inhibitor can boost the tumor-cytotoxicity effects of FGFR2 inhibitor by inhibiting PI3K/AKT and RAS/ERK pathways in FGFR2-amplified GC, and overcome FGFR2 inhibitor resistance caused by feedback activation. On the other hand, SHP2 inhibitor can activate CD8+ T cells to kill tumor cells, suggesting its synergizing effects with FGFR2 inhibitor by enhancing T cell-mediated anti-tumor immune responses. Our results demonstrate the utility and feasibility of combining SHP2 inhibitor to FGFR2 inhibitor in GC patients with FGFR2 amplification.

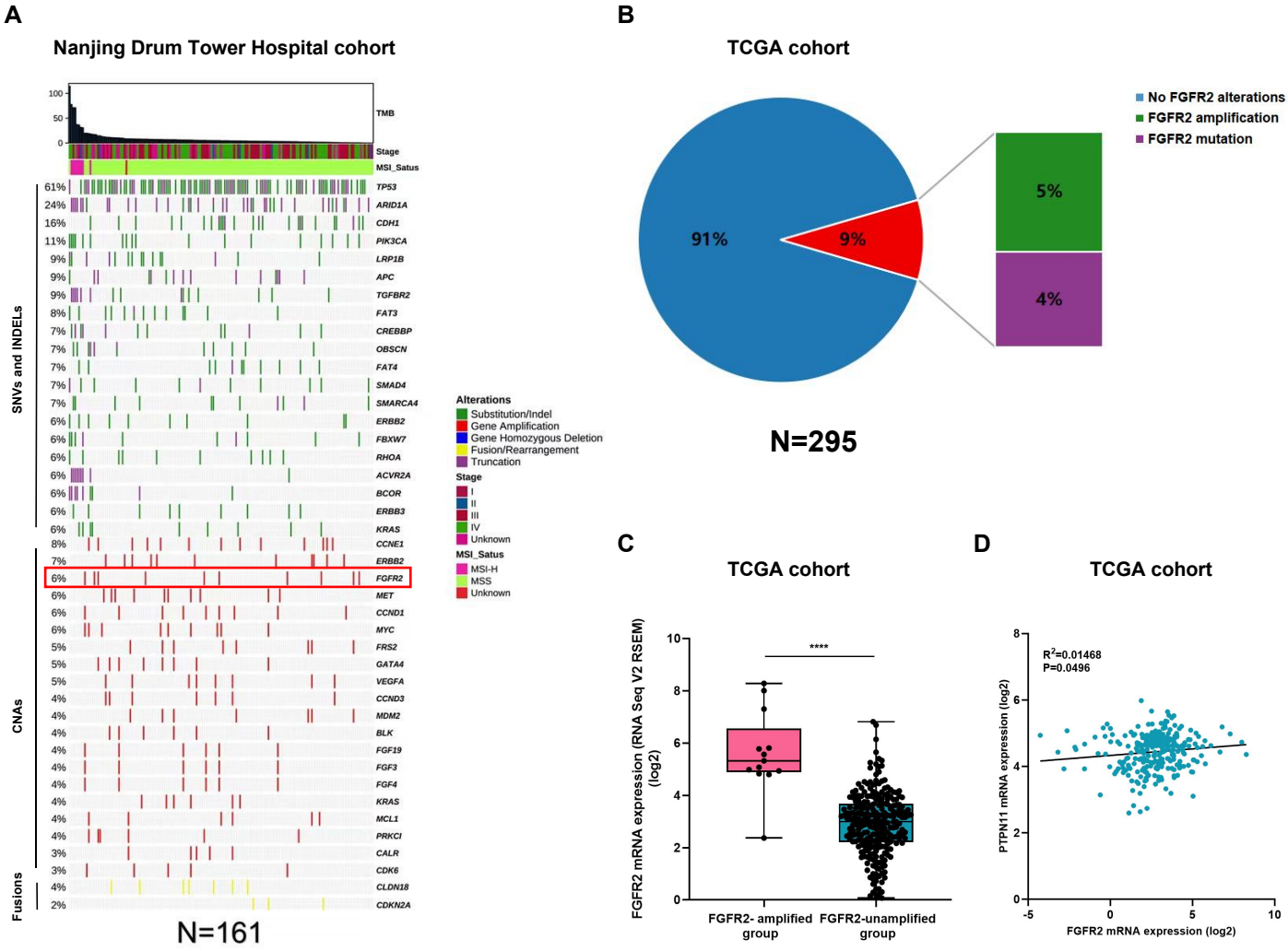
A
Nanjing Drum Tower Hospital cohort
TMB
Stage
MSI_Satus
SNVs and INDELs
CNAs
Fusions
61% TP53
24% ARID1A
16% CDH1
11% PIK3CA
9% LRP1B
9% APC
9% TGFBR2
8% FAT3
7% CREBBP
7% OBSCN
7% FAT4
7% SMAD4
7% SMARCA4
6% ERBB2
6% FBXW7
6% RHOA
6% ACVR2A
6% BCOR
6% ERBB3
6% KRAS
8% CCNE1
7% ERBB2
6% FGFR2
6% MET
6% CCND1
6% MYC
5% FRS2
5% GATA4
5% VEGFA
4% CCND3
4% MDM2
4% BLK
4% FGF19
4% FGF3
4% FGF4
4% KRAS
4% MCL1
4% PRKCI
3% CALR
3% CDK6
4% CLDN18
2% CDKN2A
N=161
Alterations
Substitution/Indel
Gene Amplification
Gene Homozygous Deletion
Fusion/Rearrangement
Truncation
Stage
I
II
III
IV
Unknown
MSI_Satus
MSI-H
MSS
Unknown
B
TCGA cohort
No FGFR2 alterations
FGFR2 amplification
FGFR2 mutation
91%
9%
5%
4%
N=295
C
TCGA cohort
FGFR2 mRNA expression (RNA Seq V2 RSEM) (log2)
****
FGFR2- amplified group
FGFR2-unamplified group
D
TCGA cohort
R2=0.01468
P=0.0496
PTPN11 mRNA expression (log2)
FGFR2 mRNA expression (log2)

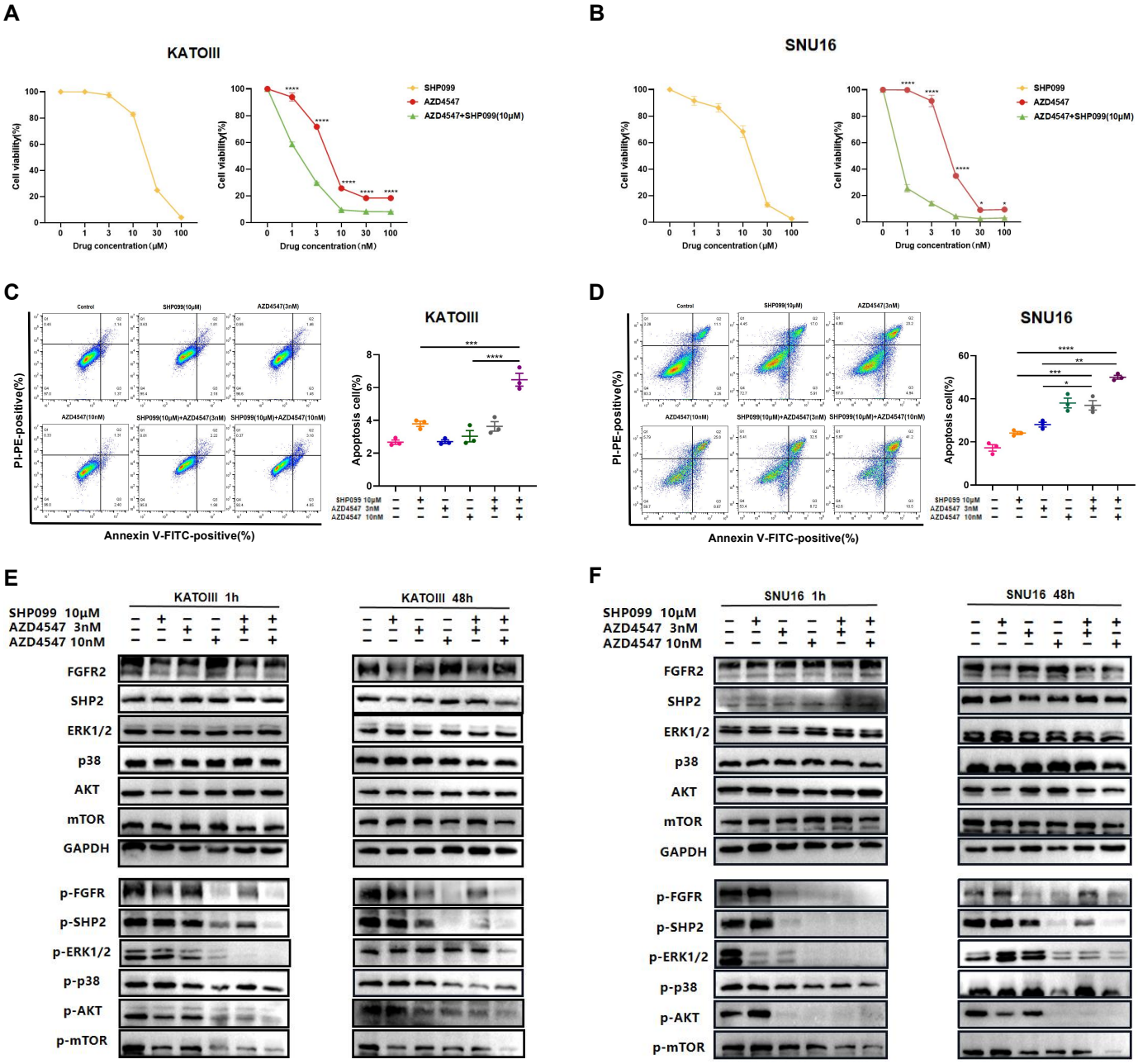
A
KATOIII
Cell viability(%)
Drug concentration（μM）
Drug concentration（nM）
SHP099
AZD4547
AZD4547+SHP099(10μM)
B
SNU16
C
KATOIII
Control
SHP099(10μM)
AZD4547(3nM)
AZD4547(10nM)
SHP099(10μM)+AZD4547(3nM)
SHP099(10μM)+AZD4547(10nM)
PI-PE-positive(%)
Annexin V-FITC-positive(%)
Apoptosis cell(%)
SHP099 10μM
AZD4547 3nM
AZD4547 10nM
D
SNU16
E
KATOIII 1h
KATOIII 48h
SHP099 10μM
AZD4547 3nM
AZD4547 10nM
FGFR2
SHP2
ERK1/2
p38
AKT
mTOR
GAPDH
p-FGFR
p-SHP2
p-ERK1/2
p-p38
p-AKT
p-mTOR
F
SNU16 1h
SNU16 48h

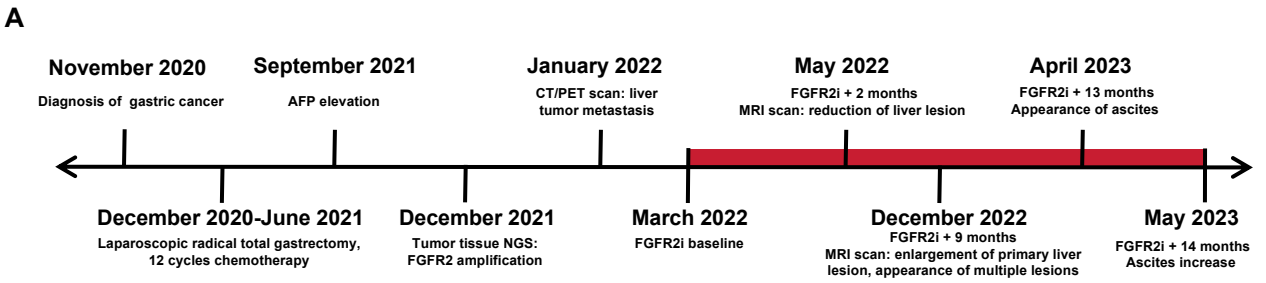
A
November 2020
Diagnosis of gastric cancer
September 2021
AFP elevation
January 2022
CT/PET scan: liver tumor metastasis
May 2022
FGFR2i + 2 months
MRI scan: reduction of liver lesion
April 2023
FGFR2i + 13 months
Appearance of ascites
December 2020-June 2021
Laparoscopic radical total gastrectomy, 12 cycles chemotherapy
December 2021
Tumor tissue NGS: FGFR2 amplification
March 2022
FGFR2i baseline
December 2022
FGFR2i + 9 months
MRI scan: enlargement of primary liver lesion, appearance of multiple lesions
May 2023
FGFR2i + 14 months
Ascites increase

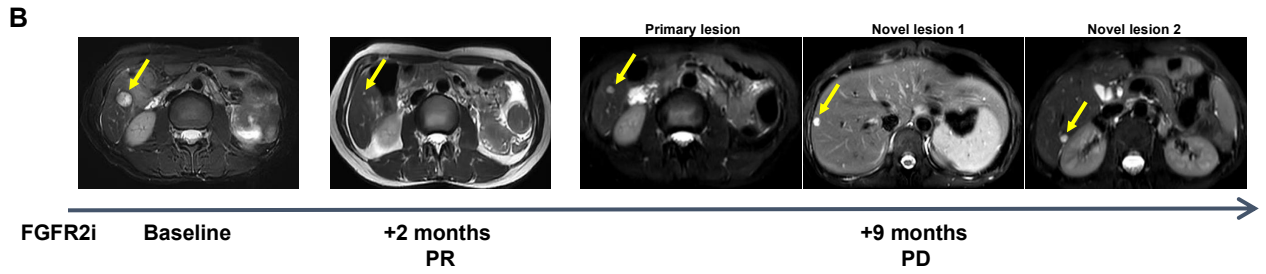
B
Primary lesion
Novel lesion 1
Novel lesion 2
FGFR2i
Baseline
+2 months
PR
+9 months
PD

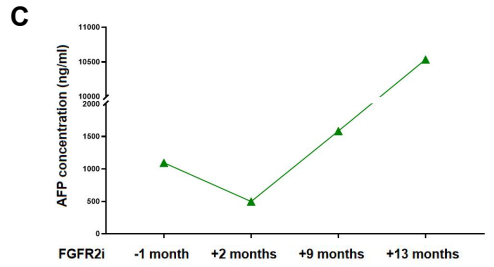
C
AFP concentration (ng/ml)
11000
10500
10000
2000
1500
1000
500
0
FGFR2i
-1 month
+2 months
+9 months
+13 months

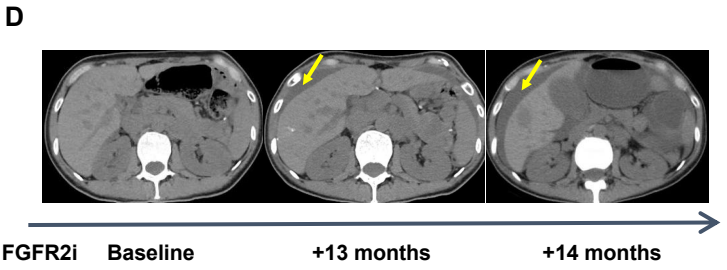
D
FGFR2i
Baseline
+13 months
+14 months

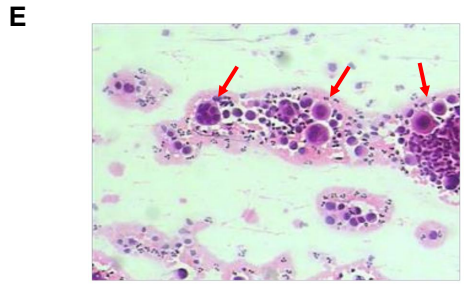
E

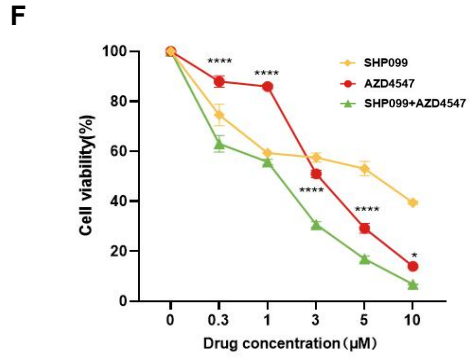
F
Cell viability(%)
100
80
60
40
20
0
0
0.3
1
3
5
10
Drug concentration (μM)
SHP099
AZD4547
SHP099+AZD4547
****
****
****
****
*

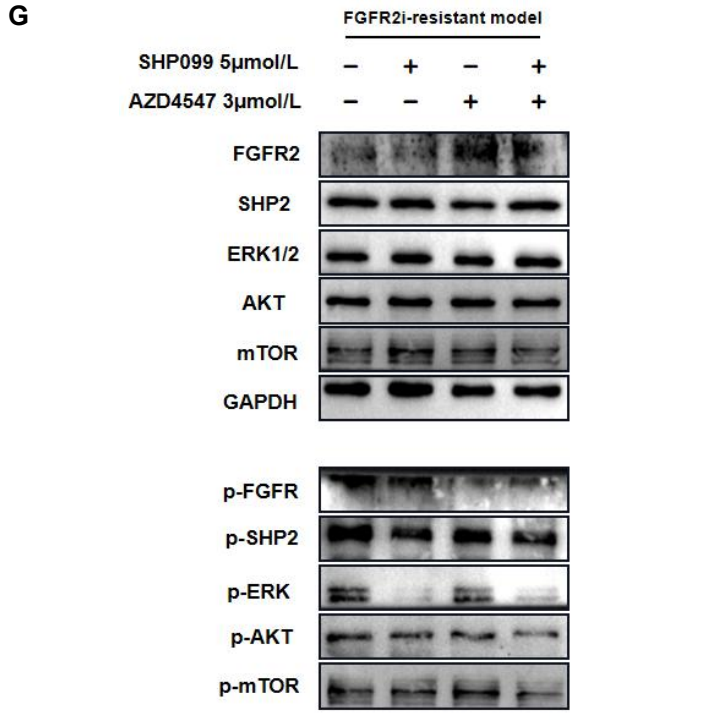
G
FGFR2i-resistant model
SHP099 5μmol/L
AZD4547 3μmol/L
FGFR2
SHP2
ERK1/2
AKT
mTOR
GAPDH
p-FGFR
p-SHP2
p-ERK
p-AKT
p-mTOR

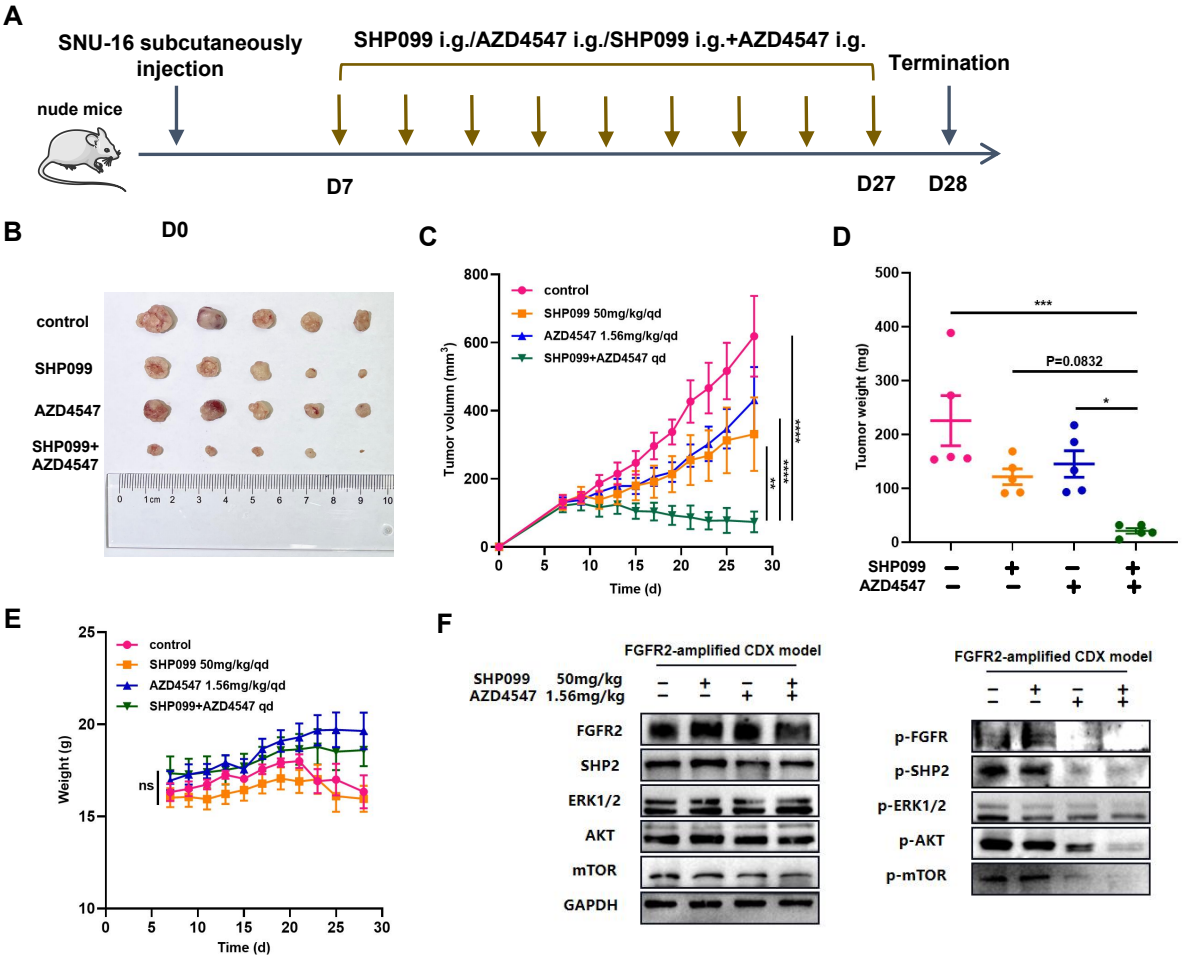
A
SNU-16 subcutaneously injection
SHP099 i.g./AZD4547 i.g./SHP099 i.g.+AZD4547 i.g.
Termination
nude mice
D7
D27
D28
B
D0
control
SHP099
AZD4547
SHP099+ AZD4547
C
control
SHP099 50mg/kg/qd
AZD4547 1.56mg/kg/qd
SHP099+AZD4547 qd
Tumor volumn (mm3)
Time (d)
D
Tuomor weight (mg)
P=0.0832
SHP099
AZD4547
E
Weight (g)
ns
Time (d)
F
FGFR2-amplified CDX model
SHP099 50mg/kg
AZD4547 1.56mg/kg
FGFR2
SHP2
ERK1/2
AKT
mTOR
GAPDH
p-FGFR
p-SHP2
p-ERK1/2
p-AKT
p-mTOR

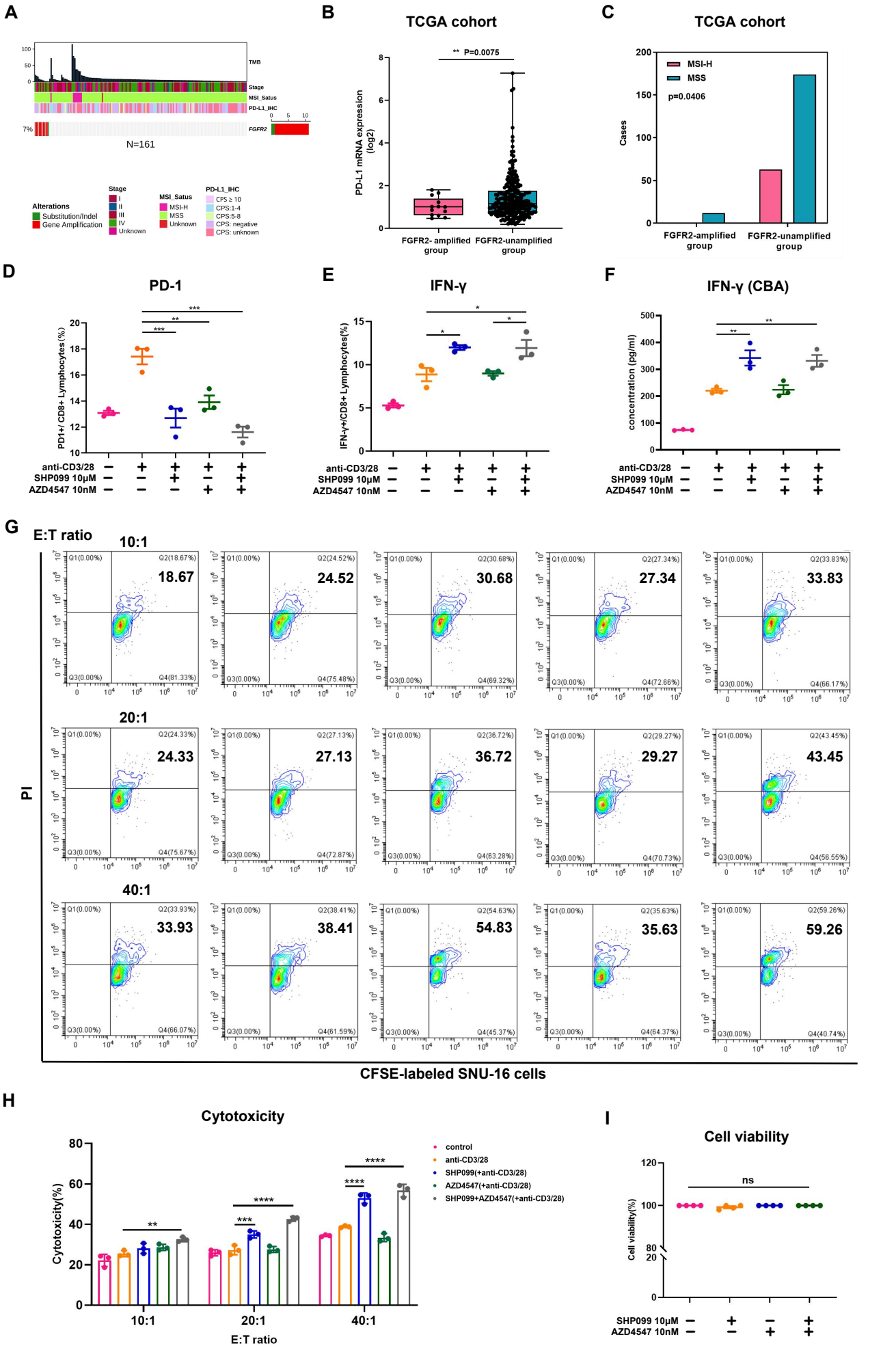
A
TMB
Stage
MSI_Satus
PD-L1_IHC
FGFR2
7%
N=161
Alterations
Substitution/Indel
Gene Amplification
Stage
I
II
III
IV
Unknown
MSI_Satus
MSI-H
MSS
Unknown
PD-L1_IHC
CPS ≥ 10
CPS:1-4
CPS:5-8
CPS: negative
CPS: unknown
B
TCGA cohort
** P=0.0075
PD-L1 mRNA expression (log2)
FGFR2- amplified group
FGFR2-unamplified group
C
TCGA cohort
MSI-H
MSS
p=0.0406
Cases
FGFR2-amplified group
FGFR2-unamplified group
D
PD-1
PD1+/ CD8+ Lymphocytes(%)
anti-CD3/28
SHP099 10μM
AZD4547 10nM
E
IFN-γ
IFN-γ+/CD8+ Lymphocytes(%)
anti-CD3/28
SHP099 10μM
AZD4547 10nM
F
IFN-γ (CBA)
concentration (pg/ml)
anti-CD3/28
SHP099 10μM
AZD4547 10nM
G
E:T ratio
10:1
18.67
24.52
30.68
27.34
33.83
20:1
24.33
27.13
36.72
29.27
43.45
40:1
33.93
38.41
54.83
35.63
59.26
PI
CFSE-labeled SNU-16 cells
H
Cytotoxicity
Cytotoxicity(%)
control
anti-CD3/28
SHP099(+anti-CD3/28)
AZD4547(+anti-CD3/28)
SHP099+AZD4547(+anti-CD3/28)
10:1
20:1
40:1
E:T ratio
I
Cell viability
ns
Cell viability(%)
SHP099 10μM
AZD4547 10nM

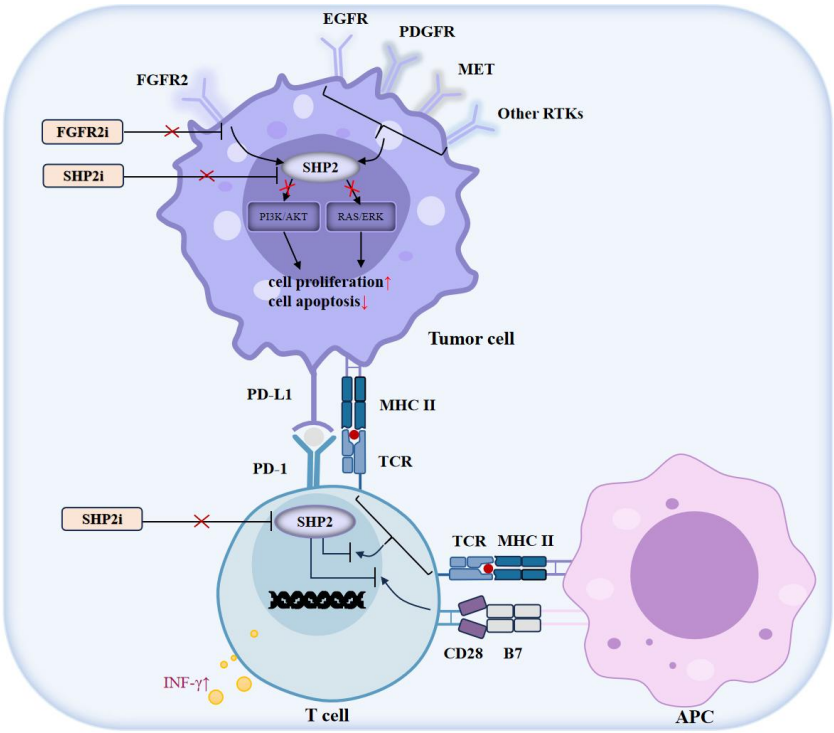
EGFR
PDGFR
MET
FGFR2
Other RTKs
FGFR2i
SHP2i
SHP2
PI3K/AKT
RAS/ERK
cell proliferation↑
cell apoptosis↓
Tumor cell
PD-L1
MHC II
PD-1
TCR
SHP2i
SHP2
TCR
MHC II
CD28
B7
INF-γ↑
T cell
APC